CHAPTER 2

Seismic Method

This chapter explains theory of the geophysical methods that focus on seismic reflection. Seismic reflection methods are well known for the exploration to achieve an image of subsurface structure. This method depends on the variation in elastic properties of medium (seismic velocity and/or bulk density). When seismic wave energy is propagating through one medium to another medium with difference elastic properties, the wave properties are changed such as amplitude, wave front, travel time and wave direction. If we detect seismic wave on the surface, then, the change in seismic properties could reveal the geological structure and the material properties.

Seismic source generates seismic wave through the elastic medium, some part of the energy is reflected to the earth's surface due to acoustic impedance contrasts which generally occurred where there is the change of lithology changes. The returning waves are recorded at the surface by sensitive instrument called receivers. The amplitudes of seismic waves were recorded as a function of the travel time (t) and offset (x) in the form of seismic traces. The seismic raw data from the field contain many signals from all the seismic waves that generated by seismic source including some noises and could not present the realistic image of the subsurface geometry for the interpretation. Therefore, seismic field data need to analyze and process before that could be used to represent the subsurface geometry. The seismic data processing is performed by a sequence of operations to extract useful information from a set of raw data. This chapter explains the reflection seismic method that used in the study area including the fundamental of seismic reflection, data acquisition, seismic data processing, and the results which will be interpreted for recognizing geological geometry. Figure 2.1 shows briefly procedure of seismic method.

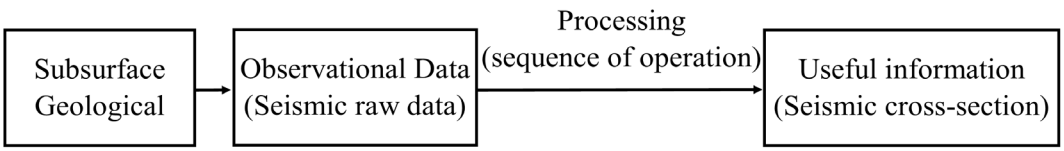

Figure 2.1 represents scheme of seismic method

2.1. Seismic wave propagation

The seismic exploration basically consists of generating seismic waves from the surface into the ground and, then, the seismic energy disturbance several types of waves propagating within the earth and along its surface. The generated waves simply can be divided into two main categories; body waves and surface waves. The body waves are transmitted through the interior of the Earth while the surface wave is traveling near the earth's surface. The body waves include with longitude waves which travel fastest and reach the surface before any anther waves called primary wave (P-wave) and transverse or shear waves (S-wave). The main characteristic of P-wave when travel in some material is that the direction of particle motion is parallel to the direction of wave propagation. While that of S-wave moves in the direction perpendicular to the wave propagation. Both seismic velocities depend on the elastic parameters as follow (Kearey and Brooks, 1991; Sheriff, 1995; Telford, Gelgart, and Sheriff, 1990)

$$V_p = \sqrt{\frac{\lambda + 2\mu}{\rho}} \tag{2.1}$$

$$V_s = \sqrt{\frac{\mu}{\rho}} \tag{2.2}$$

where λ and μ are the Lamé constants (Sheriff, 2002) and ρ is density of medium. The Lamé constants are characteristics of elastic response of a particular medium which also named as the elastic constants of that medium. In general, for elastic medium, the constants $\lambda, \mu,$ and ρ depend on several factors such as lithology (matrix and sorting), porosity, cementation, etc. The examples of seismic velocities for the typical formation are shows on Table 2..

Table 2.1 exhibits elastic wave velocities and densities in typical formation (Bourbié, Coussy, and Zinszner, 1987)

Typical formation	P-wave velocity (m/s)	S-wave velocity (m/s)	Density (g/cm^3)
Soil	300-700	100-300	1.7-2.4
Dry sands (loose)	400-1200	100-500	1.5-1.7
Wet sands	1500-2000	400-600	1.9-2.1
Near-surface sand and gravel	400-2300	100-700	1.5-2.2
Saturated sandstones	2000-3500	800-1800	2.1-2.4
Limestones	3500-6000	2000-3300	2.4-2.7
Basalt	5500-6500	2800-3400	2.7-3.1
water	1450-1500	-	1

2.1.1. Seismic waves travel times

The seismic energy is introduced into the ground and when it encounters the interface between ground layers, it will reflect and refract follow the Snell's law (Yilmaz, 2001). The reflected and refracted waves are traveling black to the surface and detected by the group of receivers. The seismic waves are recorded as a function of the travel time (t) and offset (x) in the seismic traces. Figure 2.2 exhibits seismic wave ray-paths in the simplest case, a single horizontal layer overlay the half-space medium. The seismic waves travel from shot point (S) to the receiver location (R) with three different ray-paths. The directed wave (red ray-path) travels from shot direct to receiver. The refracted wave (green ray-path) travels from shot location encounter interface with critical angle and refracts along the interface, then, refracts back to receiver at the surface. The reflected wave (blue ray-path) travels from shot location encounter interface and reflects black to the receiver at the surface. This study focuses on reflected waves. Consequently, other waves are considered as noise in data analysis. The characteristic of each wave can be recognized because of their expression on seismic travel time curves in Figure 2.3.

The travel time of directed wave that travelling a certain distance x along the surface depends only on the wave velocity v_1, the velocity of the horizontal layer. On a time-

distance graph, the directed wave is represented by a straight line though the origin with a slope of $1/v_1$, red line in Figure 2.3.

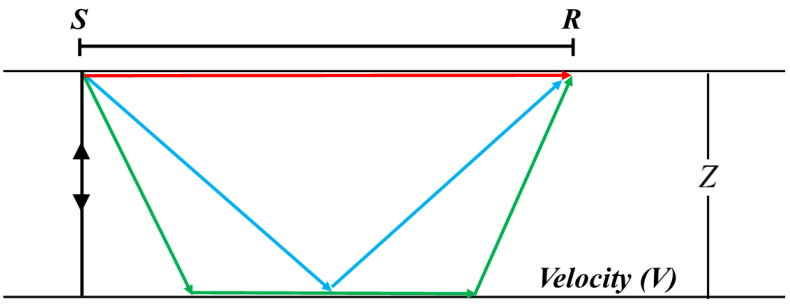

Figure 2.2 exhibits seismic wave ray-paths in the simplest model, a single horizontal layer overlay the half-space medium. The directed, refracted, and reflected waves are represented with red, blue, and green lines, respectively.

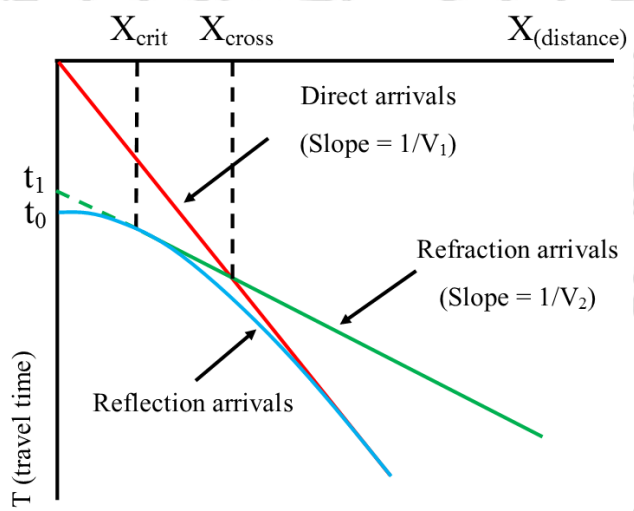

Figure 2.3 illustrates the travel time curves of directed, refracted, and reflected waves in red, green and blue lines, respectively.

The refracted wave only occurs when velocity of the underlaid layer (v_2) is higher than that of the horizontal layer, $v_2 > v_1$, and the incident wave reaches the boundary at the critical angle. The travel time of refracted wave is presented in Figure 2.3 by green straight line with a slope of $1/v_2$ which intersects the t-axis at a time t_1.

The reflected wave is represented by a hyperbola on the time-distance graph. Its peak, t_0, is at the zero offset ($x = 0$) as seismic wave is incident normal to the interface. The

increase of travel time depends on offset x and velocity v_1. The t_0 point is very important as a basic concept of normal moveout correction. The travel time of reflected wave is

$$t_x = \sqrt{t_0^2 + \frac{x^2}{v_1^2}} \tag{2.3}$$

where

$$t_0 = 2\frac{z}{v_1} \tag{2.4}$$

and the approximate

$$t_x \approx t_0\left(1 + \frac{x^2}{2v_1^2 t_0^2}\right) = t_0 + \frac{x^2}{2v_1^2 t_0} \tag{2.5}$$

when x is the horizontal distance (offset) between source and receiver position, v_1 is the velocity of the medium above reflecting interface, t_0 is zero-offset travel time, and t_x is travel time at any offset x.

2.1.2. Reflection and transmission coefficients

When seismic waves propagate though subsurface and reach the boundary between layers where there is a contrast in acoustic impedance (Z), velocity times density. The wave's energy is partitioning by reflection and transmission. In the case of the normal incident P-wave (Figure 2.4), the tangential displacement is zero. Therefore, the equation of reflection (R) and transmission (T) coefficients are (Telford, Gelgart, and Sheriff, 1990).

$$R = \frac{A_r}{A_0} = \frac{v_2\rho_2 - v_1\rho_1}{v_2\rho_2 + v_1\rho_1} = \frac{Z_2 - Z_1}{Z_2 + Z_1} \tag{2.6}$$

$$T = \frac{A_t}{A_0} = \frac{2v_1\rho_1}{v_2\rho_2 + v_1\rho_1} = \frac{2Z_1}{Z_2 + Z_1} \tag{2.7}$$

where Z is acoustic impedance, product of density ρ and velocity v, for each layer labeled by subscripted number. The $A_0, A_r,$ and A_t are the amplitude of the incident, reflected, and transmitted waves, respectively.

Generally, the harder rock has greater acoustic impedance. For seismic waves to propagate most of their energy efficiently across a boundary, the acoustic impedance contrast should be small. If the high contrast of the acoustic impedance is encountered, most of the wave energy will be reflected and less energy would have transmitted. This

might be the problem for the reflection methods when the high velocity zone is found at shallow or near the surface.

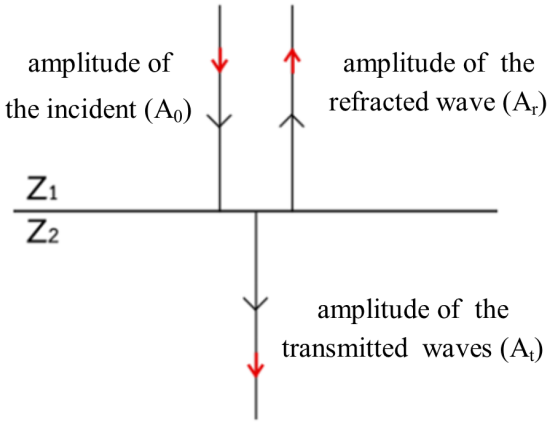

Figure 2.4 shows the normal incident P-wave generates reflected and transmitted P-waves (Kearey and Brooks, 1991).

2.2. Essential concepts for reflection data processing

The data processing is approached to extract useful information from a set of raw data. The seismic reflection data from the field survey do not represent underground structure directly. The field data need to be edited, modified, or transformed with specific procedures called seismic reflection data processing to provide the final seismic section that will be represented an image of subsurface. This topic will focus on the concept of each procedure such as, amplitude attenuation and gain recovery, static correction, frequency filter, F-K filter, surface consistence deconvolution, normal move out correction, and velocity analysis and stacking.

2.2.1. Amplitude attenuation and gain recovery

The traveling wave will suffer from amplitude decay due to at least three factors: geometrical spreading with distance, absorption of energy in medium, and partial transmission and reflection loss at the boundary layer (Telford, Gelgart, and Sheriff, 1990).

The wave energy (E) is proportionally with the power of two of wave's amplitude ($E \propto A^2$). For a seismic point source at the surface which generates the spherical wave, when

seismic wave propagates deeper thought the earth its wavefront cover the larger area with hemisphere shape, its energy intensity ($I = E/wavefront\ surface\ area$) will be decreased proportionally with distance square (r^2) from the source.

$$I = \frac{E}{4\pi r^2} \quad \rightarrow \quad I \propto \frac{1}{r^2} \tag{2.8}$$

The intensity of seismic wave is directly related to wave energy. Therefore, the amplitude of wave will be effected by the spherical divergence as

$$E \propto \frac{1}{r^2} \quad \rightarrow \quad A \propto \frac{1}{r} \tag{2.9}$$

This mean that the effect of geometrical spreading will cause variation of the wave amplitude with distance.

Concerning with wave ray-path, energy of the wave is lost during travelling because of its transit through the earth. The lost energy is transformed into other forms of energy, usually heat due to absorption process by inelastic and inhomogeneous mediums (Telford, Gelgart, and Sheriff, 1990). The loss energy by absorption can be expressed in terms of amplitude that given by

$$A = A_0 e^{-\eta x} \tag{2.10}$$

where A_0 is the initial amplitude of the wave at the reference point, A is the amplitude at a displacement x from the reference location, and η is absorption coefficient.

In order to recover the amplitude of the signal at deeper depth, it is commonly to apply exponential gain function which approximated for the amplitude attenuation losses (Telford, Gelgart, and Sheriff, 1990). The exponential gain recovery works by multiplying the traces by an exponential function as

$$\text{Gain recovery } = te^{nt} \tag{2.11}$$

where t is two-ways travel time, n is the constant value that implies a value of exponential (t) for the multiplier to be used on the sample at that time.

2.2.2. Static correction

For a horizontal reflector, if the earth surface is irregular surface and the near surface layers velocity variation, as always be in the real field acquisition, the reflected waves pattern in different traces will not line in a perfect hyperbola form. Figure 2.5a shows that the difference between the elevations of the sources and receivers, or the variation of near surface velocities make the seismic wave travels with slightly different lengths of the raypaths therefore there are the small time shifts in each trace. The static correction is the time shift adjustment for each trace in such a way that the sources and receivers will be presented at the reference datum. The elevation static correction is compensated for the effect of topography to adjust the source and receiver elevation to the reference datum. The refraction static correction is compensated for the weathering layer. After static correction, the reflector should be appeared along the hyperbola curve (Figure 2.5b).

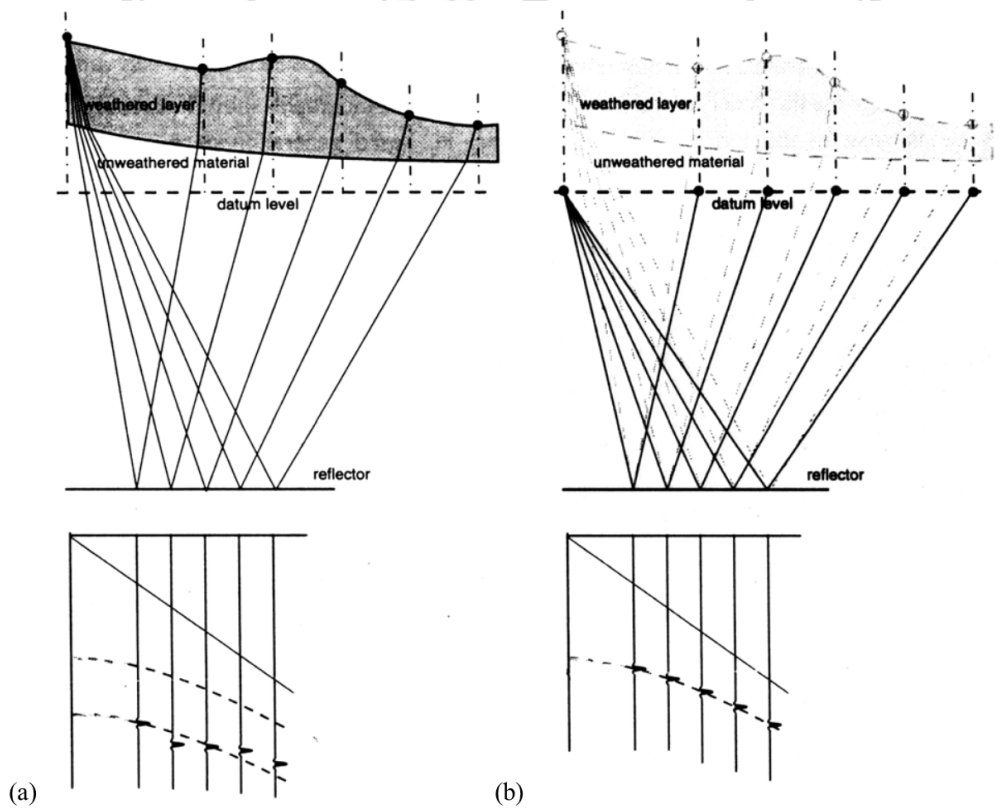

Figure 2.5 shows that (a) the reflectors are not lying in hyperbola cause by the effect of surface topography and weathered layer velocity variation and (b) the reflector is lying in hyperbola after applied static correction (Brouwer and Helbig, 1998).

2.2.3. Frequency filter

The application of frequency-filter requires data in frequency domain (amplitude as a function of frequency or amplitude spectrum) by Fourier Transform. Frequency domain filter involves multiplying the amplitude spectrum of input seismic traces by the filter operator. After that, the data in frequency domain converse back into time domain by inversed Fourier Transform. The frequency filters are classified in form of band-pass, low-pass, and high-pass. The objective of this filter is to remove noise that it is not exist a frequency signal range. The band-pass filter is most commonly used, because a seismic trace typically contains some low-frequency noise, such as ground roll, and some high-frequency ambient noise. In designing a band-pass filter, the objective is to pass a certain of bandwidth and to remove outside of bandwidth (Figure 2.6a). The filter operator that required for this objective (Yilmaz, 2001) is giving by

$$A(f) = \begin{cases} 1, & f_2 < f < f_3 \\ 0, & \text{otherwise} \end{cases} \tag{2.12}$$

where f_2 and f_3 are low and high cut of bandwidth frequency. The reason of principle of ringing which occurs in time domain when sharp boundaries are present in the frequency domain (Figure 2.6 a and b). Consequently, to remove ringing effect in the result, it need rump function at both low and high edges as f_1 and f_4 (Figure 2.6 c and d).

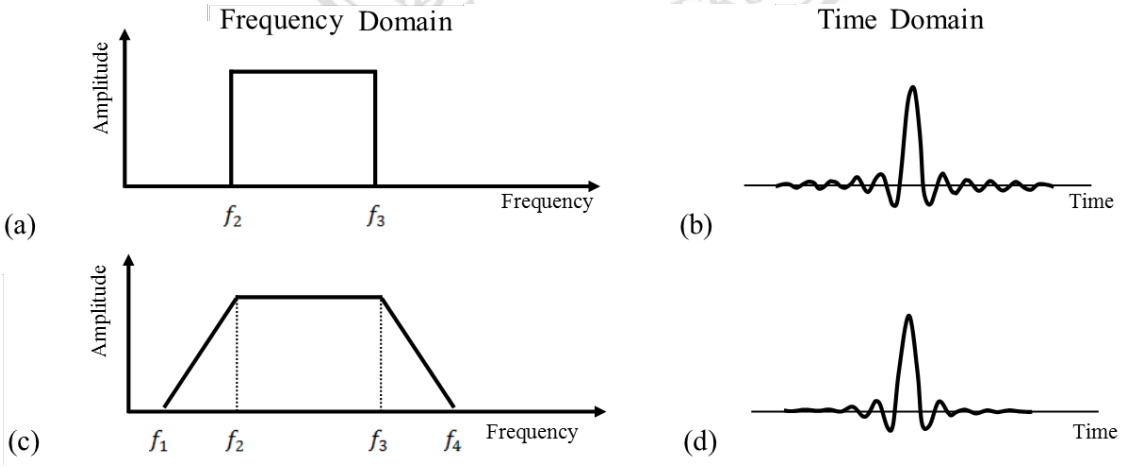

Figure 2.6 demonstrates (a) sharp boundaries in frequency domain cause (b) ringing artifact in time domain and (c) window of band-pass filter, f_2-f_3, and f_1 and f_4 as ramps functions to remove ringing effect in time domain (d) resulted from optimum operator filter (Kearey and Brooks, 1991).

2.2.4. F-K filter

The F-K filter is a tool that applied to the seismic data in the frequency-wavenumber domain. The objective of this filter is to eliminate the coherent linear noise (ground roll and air wave) and side-scattered energy from the reflection energy in F-K domain. Input seismic record is converted from time and space sampled traces into the F-K domain by the two-dimensional Fourier Transform. Figure 2.7b illustrates the various types of energy in F-K domain from shot gather (Figure 2.7a). The different type of seismic energy separates within different zone in F-K spectrum. This provides us the ability to design or to zero out the unwanted signal based on the apparent velocity or the slope in F-K spectrum plot. The F-K filter will be designed and then multiplied with F-K domain of seismic record. After that, the filtered F-K spectrum is converted back to time-space domain by the inverse Fourier Transform into the form of the seismic traces. A significant parameter of this step is the window or range of the filter spectrum that will pass the wanted signal or zero out the energy of the unwanted signal in F-K spectrum (Harris and White, 1997; Jeng, 1995).

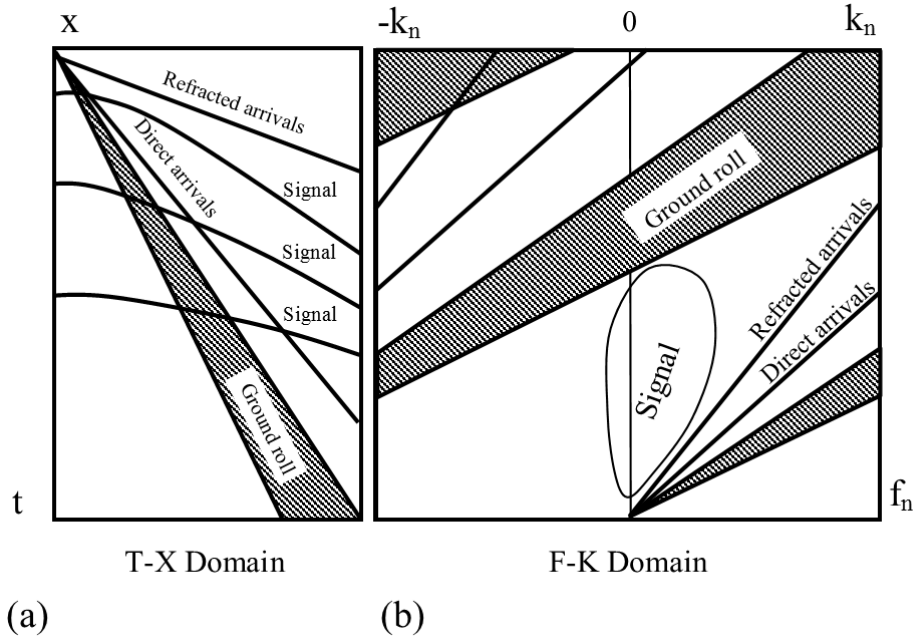

Figure 2.7 illustrates (a) common sketch of shot gather in time and offset domain and (b) its frequency-wavenumber spectrum plot, the reflection events (wanted signals) and different types of noise (linear events) will be separated and easy to identify.

2.2.5. Surface Consistent Deconvolution

Deconvolution compress the basic wavelet in the recorded seismogram, attenuates reverberation and short-period multiple, thus increase temporal resolution and yields a representation of subsurface reflectivity. To understand deconvolution, the constituent element of recorded seismic are examined. The ideal seismic trace $S(t)$ is modelled by the convolution $(*)$ of the reflectivity function $R(t)$ with composite input or source wavelet $W(t)$, Figure 2.8. This source wavelet has many component, including source signature, recording filter, surface reflections, and receiver-array response (Kearey and Brooks, 1991).

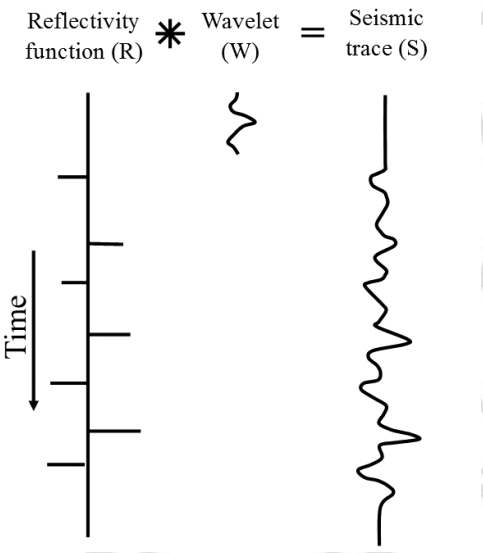

Figure 2.8 displays reflection seismogram viewed as convolution between reflectivity function and source wavelet (Kearey and Brooks, 1991).

In order to yield the reflectivity, the wavelet compression can be done using a Wiener filter $(W(t)^{-1})$. The Wiener filter shape similar inverse filter can be designed to convert the seismic wavelet into a spike, called deconvolution. The Wiener filter design is achieved using autocorrelation (Yilmaz, 2001). Autocorrelation is the correlation of a seismic waveform with itself. Since the source wavelet is unknown in practice, the amplitude spectrum of seismic trace autocorrelation is used as an alternative approximation. There are many types of deconvolution method such as spike and predictive deconvolutions. Predictive Deconvolution is the most common procedure that tries to evaluate and eliminate the predictable parts of a seismic trace (usually multiples).

Predictive deconvolution can also be used to increase resolution by altering wavelet shape and amplitude spectrum. Spiking deconvolution is a special case where the gap is set to one sample and the resulting phase spectrum is zero. The seismic trace usually can be decomposed into the convolutional effects of source, receiver, offset, and the reflectivity function response, thus causing the variations of wavelet shape affected by near-source and near-receiver conditions and source-receiver separation (Yilmaz, 2001).

Surface consistent deconvolution corrects for variation in amplitude, phase and frequency caused by inconsistent instrument responses, poor coupling, and near-surface properties (Cary and Lorentz, 1993). Surface consistent predictive deconvolution is chosen for applying to the data in this study for compressing the multiple reflectors. The four-component surface consistent deconvolution are relative fast algorithm to carries out the decomposition into log-amplitude into four-component with the Gauss-Seidal iterative inversion equation. When performing four-component surface-consistent deconvolution, it is assumed that the decomposition of amplitude spectra into source, receiver, offset, and common-depth-point components.

The source component collects effects of the source signature and near-source structural effects, and that the receiver component collects receiver characteristics and near-receiver structural effects. The offset and CDP component collect the effect of raypath from source to reflector to receiver. In addition, the magnitude of CDP component is small compared to the other components and the magnitude of the offset component due to ground roll are larger than anywhere else in other components. The assumption of surface-consistent implies that the basic wavelet shape depends only on the source and receiver location, and not on the detail of the raypath from source to reflector to receiver (Yilmaz, 2001). Consequently, deconvolution filters should be constructed from the source and receiver components, while the offset and CDP components are discarded. These ensures that traces from the same surface source and receiver location have the same, consistent, deconvolution operator applied.

2.2.6. Normal move out correction

The seismic processing, conventionally is done in common midpoint gather. The seismic data are sorted into common midpoint (CMP) gather base on the mid-point between source and receiver, a halfway between the source and receiver, (Figure 2.9a). The reflector is represented by the hyperbola curves on time verses offset graph (Figure 2.9b). The minimum travel time t_0 is occured when the reflected wave makes a normal incidence at the interface or at zero offset ($x = 0$) for horizontal interface. The slope of hyperbola equals to zero at zero offset and increases with the offset. The increment of the travel time (t_x) depend on offset (x) and layer velocity,(2.3). Consider a reflection event on CMP gather, the normal moveout (NMO) correction is applied to remove the travel time difference that influence from the offset. The NMO correction is normally termed Δt, as the difference between the actual travel time (t_x) and the zero-offset travel time (t_0). The NMO equation is given as

$$NMO = \Delta t = t_x - t_0 \approx \frac{x^2}{2v^2 t_0} \qquad (2.13)$$

where v is the average velocity of the reflector.

Therefore, the NMO correction is depending on the offset x and velocity v that causes the time shift Δt different along traces in the same CMP gather. The NMO correction moves the hyperbola curves into horizontal events, then, the NMO-corrected traces are summed to obtain a stack trace at the particular CMP location (Figure 2.10) (Telford, Gelgart, and Sheriff, 1990).

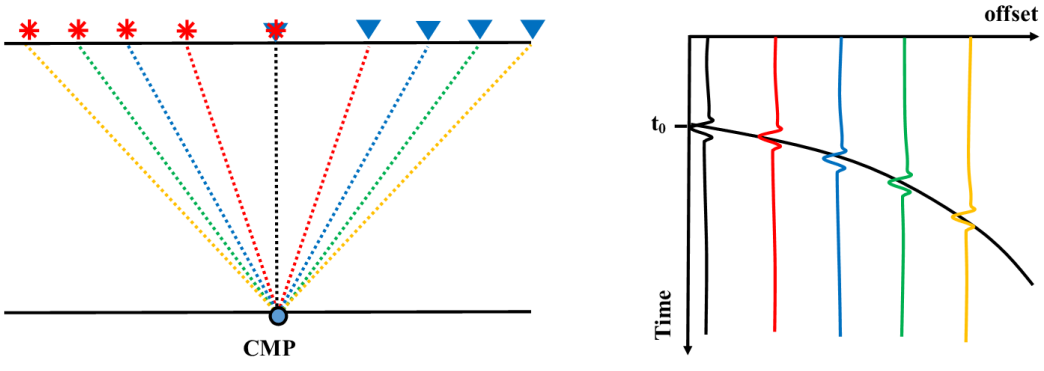

(a) (b)

Figure 2.9 shows (a) seismic raypaths associated with a single CMP gather and (b) corresponding hyperbola travel time curve for a horizontal reflector.

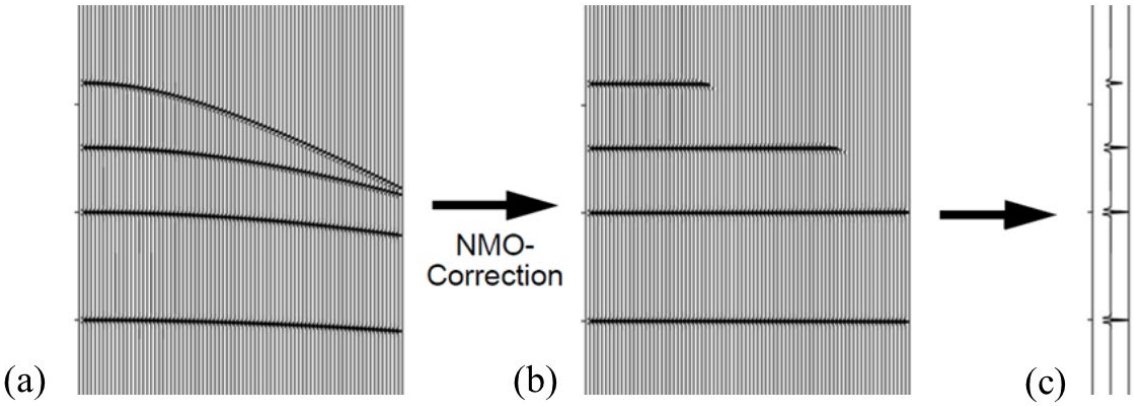

Figure 2.10 reveals the principle of NMO correction, reflections showed as (a) hyperbolas traveltime curves are moved up with correct velocities (b) aligned horizontally and then (c) stacked to improve the signal to noise ratio.

However, the earth modal has many horizontal layers, in each layer, seismic waves will travel with a certain transit time (Δt_i) and interval velocity ($v_{int,i}$), the formation velocity. The reflection hyperbolic curve concerns the velocity of medium above reflecting interface. The velocity that is used to remove the effect of NMO is called stacking velocity. The stacking velocity could be modeled as the average velocity above the reflector. The common average method that suitable for stacking velocity is a root-mean-square velocity (v_{rms}) that is an approximate seismic velocity for NMO correction. The velocity that best flattens the reflection hyperbola is also the best velocity for NMO correction. The study area has the maximum offset small compared with the reflector depth, the stacking velocity closely approximated by the v_{rms} function, (Yilmaz, 2001; Sheriff, 1995), and defined as

$$v_{rms,n} = \sqrt{\frac{\sum_{i=1}^{n} v_{int,i}^2 \Delta t_i}{t_n}} \qquad (2.14)$$

where $v_{int,i}$ is interval velocity of the i^{th} layer, Δt_i is two way zero-offset travel time through i^{th} layer, $t_n = \sum_{i=1}^{n} \Delta t_i$ is total two way zero-offset travel time, and n is the reflector number. To calculate the interval velocities from the v_{rms} the Dix conversion (Dix, 1955) is used.

$$v_{int} = \sqrt{\frac{v_{rms,n}^2 t_n - v_{rms,n-1}^2 t_{n-1}}{t_n - t_{n-1}}} \quad (2.15)$$

where v_{int} is interval velocity within the layer bounded by the $(n-1)th$ layer boundary above and nth layer boundary below, t_n and t_{n-1} are the two way zero-offset times.

2.2.7. Velocity analysis

The velocity analysis is the process of finding the stacking velocity to use for NMO correction that mention above. The common tools for helping velocity picking are velocity spectrum (Semblance) and constant velocity stack (CVS) (Yilmaz, 2001; Sheriff, 1995).

The velocity spectrum is a method that maps the selected CMP gather from offset-time domain into velocity-time domain, the stacking velocity versus two-way zero-offset domain. The NMO correction is applied to an input CMP gather using a range of constant velocity. The NMO-corrected gather is then stacked and the resultant stack traces from each constant velocity are displayed as the color density map called semblance velocity spectrum (Figure 2.11b). The correct stacking velocity will display with the higher magnitude on semblance spectrum.

Each CVS panel is a small part of stacked traces from the neighbor CMP gather that using constant stacking velocity for NMO corrected. Several trial velocities values are used and display as panel for each difference stacking velocity (Figure 2.11c). The constant velocity used in CVS method should be considered from the range of velocity need to stack the seismic data. The velocity that best flattens the reflection hyperbola is also the best velocity for NMO correction.

The stacking velocity (v_{stk}) for each reflector of selected CMP will be picked base on both velocity spectrum and CVS panels call stacking velocity function, v_{stk} versus time function chosen from the best magnitude in semblance and CVS.

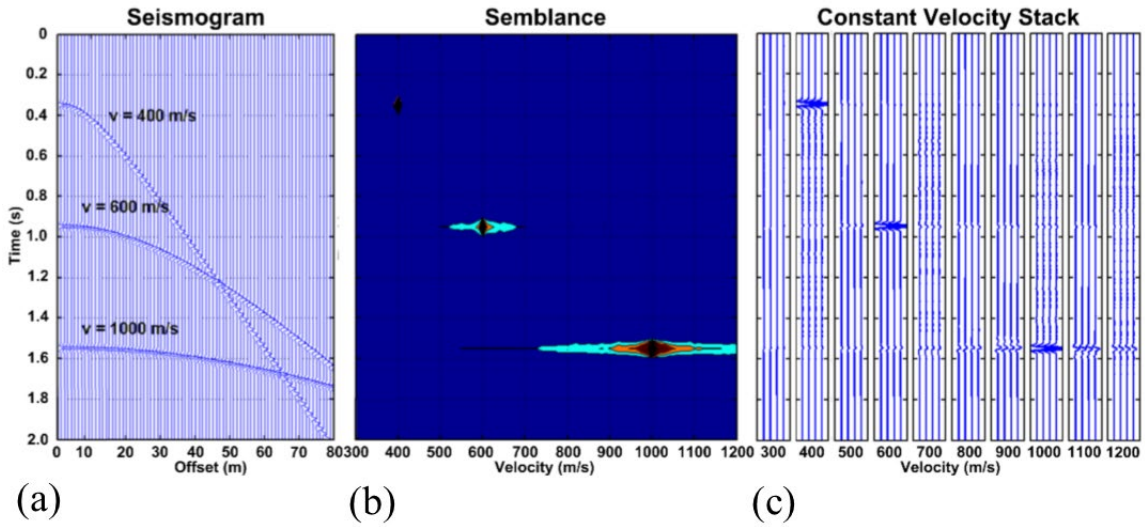

Figure 2.11 displays velocity analysis with (a) input CMP offset gather, (b) velocity spectrum and (c) constant velocity stack (Suklim, 2014)

2.3. Seismic Acquisition

The four seismic reflection survey were conducted in April to December 2015 name MO-1, MO-2, MO-3 and, MO-4 in Figure 2.12. The Differential Global Position System (DGPS) was employed to investigate accurately the geometry location of each shot and receiver station. Each shot gathers were acquired with three to five times to improved signal to noise ratio by depressing the incoherence noise. The main acquisition instruments consist of seismic source, receivers, and recorder system.

Source: The elastic wave generator (EWG) with 300 kg weight drop was used, Figure 2.13a. Seismic wave generates by dropping the 300 kg weight from 1.5 m above to the surface. An elastic band attach to EWG is used to accelerate the weight drop to increase the seismic energy. However, EWG is usually producing an effect of time delay and long wave train energy. The 20 lb sledge hammer, (Figure 2.13b), is simply the impulsive source type was also used.

Receiver: The seventy-two of 28Hz frequency response vertical geophones (Figure 2.13c) and 3 seismic cables (24 channels per cable) with maximum interval 5 m were used. When seismic energy was released. The vertical ground movement is detected by vertical single geophone. The relative motion between the coil and magnetic field in geophone generate a small electric current and recorded as seismic signal.

Recorder: The multichannel seismographs that used in this study are three Geode™ systems (Geometrics, 2017) with the maximum of 72 channels (Figure 2.13d). Geode™ is the small seismic recorder which sampling seismic analog signal from ground motion and send that through connection cable and save as the digital file in laptop personal computer.

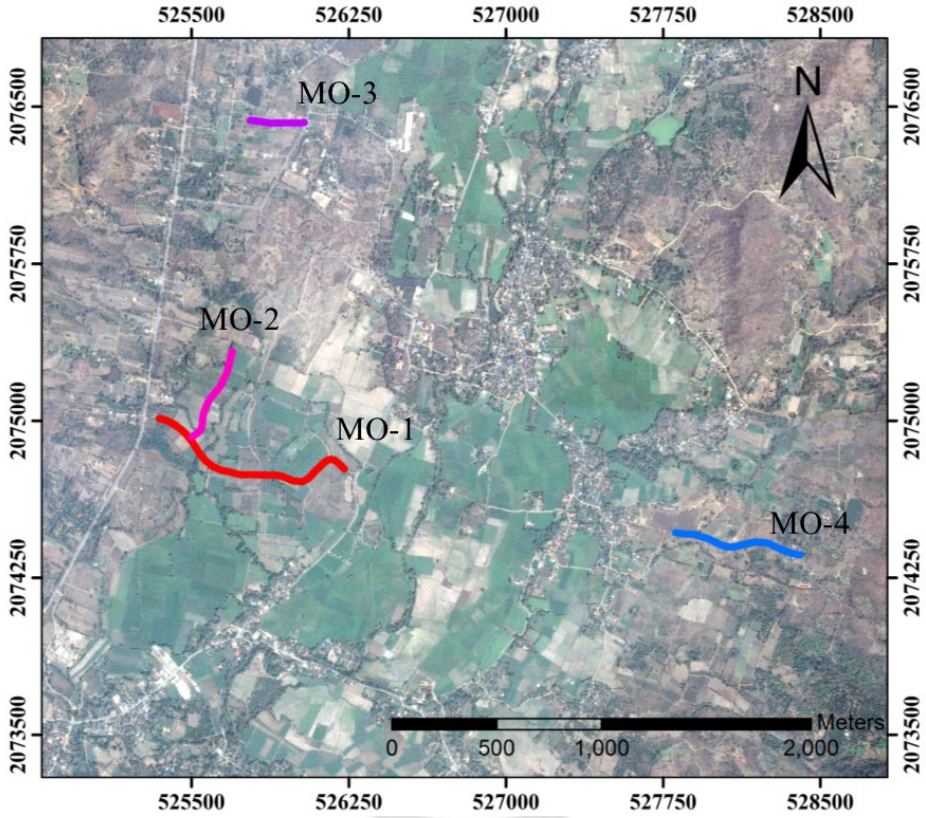

Figure 2.12 indicates the location of seismic reflection survey Lines, MO-1, MO-2, MO-3, and MO-4 shown in red, pink, purple, and blue lines, respectively, modify from (Google Earth Pro, 2013), the data from Line MO-2 are used for processing display.

There are commonly used techniques to increase quality of shallow seismic data. To determine the optimum parameter, before starting a seismic survey, it is necessary to perform field parameter test in order to set up the optimum parameters. The optimum parameters which are tested for seismic acquisition in this study are brief in Table 2. The vertical stack technique is able to enhance the signal to noise ratio in acquisition part. This study took about three to five shots at the same shot location. The total recording time is 2 s with sample interval 1 ms, the maximum frequency of sampling interval is 500Hz.

The acquisition procedures were design to mix configuration. The surface stacking chart, Figure 2.14, Figure 2.15, Figure 2.16, and Figure 2.17 show survey configuration of Line MO-1, MO-2, MO-3, and MO-4, respectively. The pattern A is split-spread configuration. To enhance the fold coverage at the start and end of the survey line, the pattern B, end-on configuration, was applied.

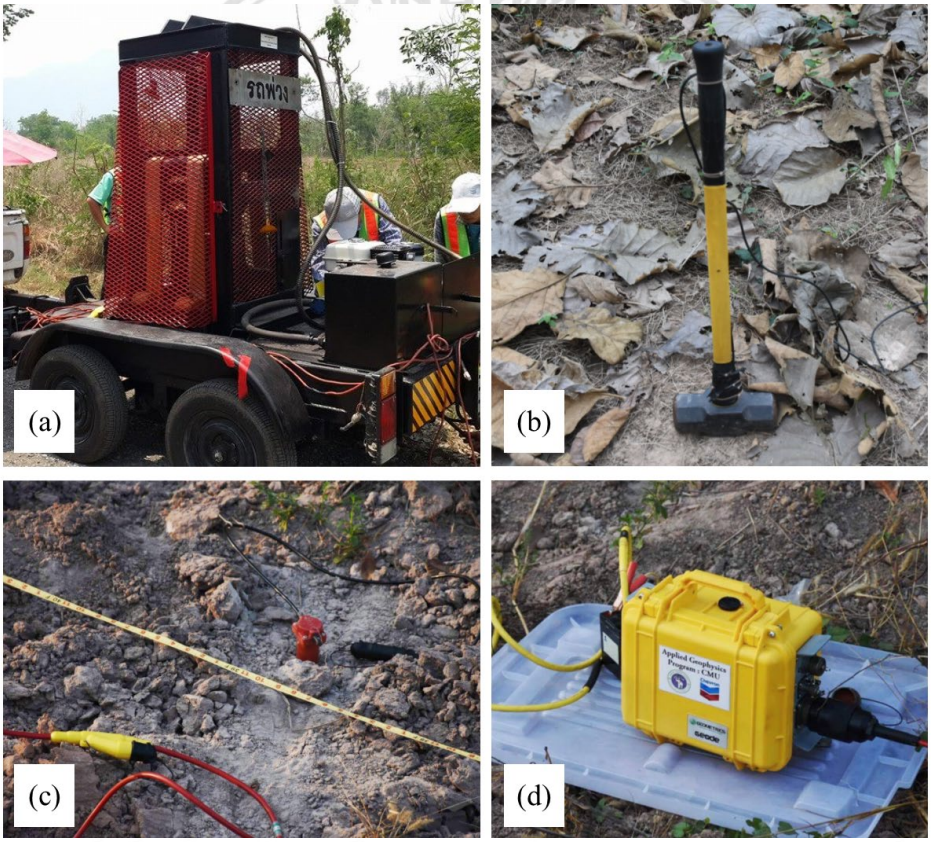

Figure 2.13 illustrates seismic equipment (a) elastic wave generator (EWG), (b) hammer 20lb, (c) single geophone and seismic cable (red cable) and (d) Geode^{TM} the acquisition system (Geometrics, 2017).

Table 2.2 shows acquisition parameters of survey Line MO-1, MO-2, MO-3 and MO-4

Item	MO-1	MO-2	MO-3	MO-4
Source	EWG	Hammer	Hammer	Hammer
Receiver	28-Hz Vertical single geophones (72 Channel)			
Geophone spacing (m)	4	4	2	5
Source spacing (m)	4	4	2	5
Vertical stack	No	Yes	Yes	Partial
Number of vertical stack	1	5	5	1-5
Sampling rate (ms)	1			
Record length (s)	2			
Binning size	2	1.96	1	2.43
Number of CMP	515	230	248	239
Surface line (m)	1030	450	248	578

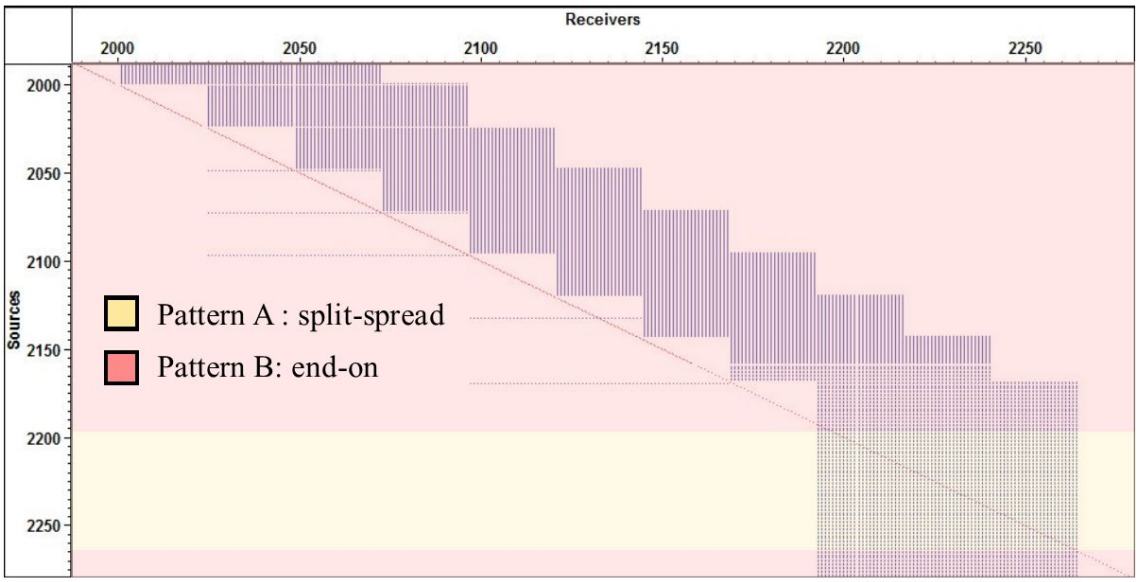

Figure 2.14 shows stacking chart of survey Line MO-1 (red and blue dots are shot and receiver locations) with split-spread configuration (yellow zone) and end-on configuration (light-red zone).

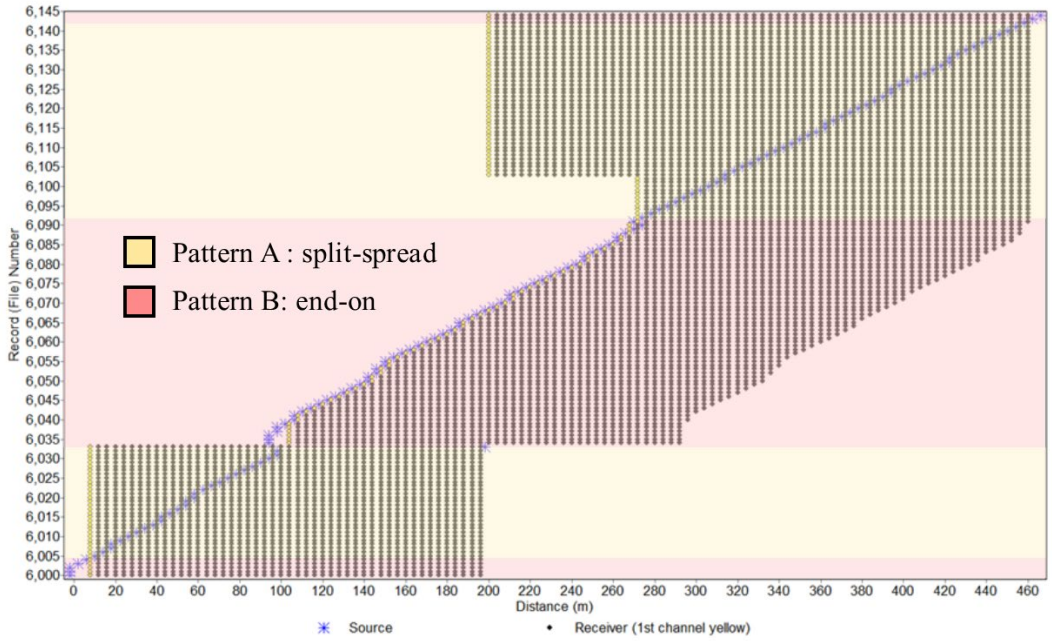

Figure 2.15 shows stacking chart of survey Line MO-2 (blue star and black dot are shot and receiver locations) with split-spread configuration (yellow zone) and end-on configuration (light-red zone).

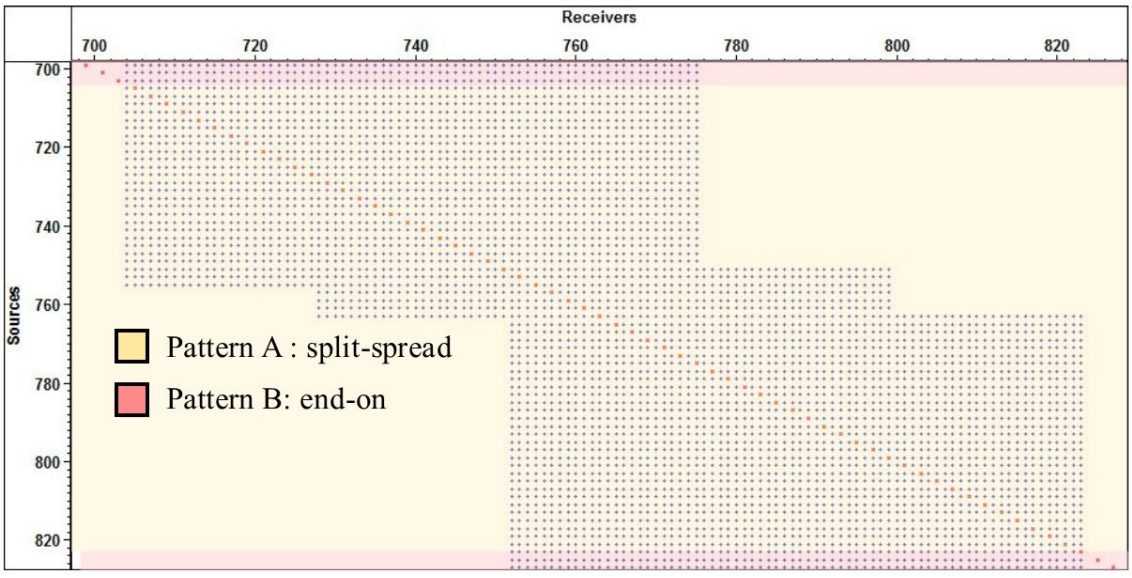

Figure 2.16 shows stacking chart of survey Line MO-3 (red and blue dots are shot and receiver locations) with split-spread configuration (yellow zone) and end-on configuration (light-red zone).

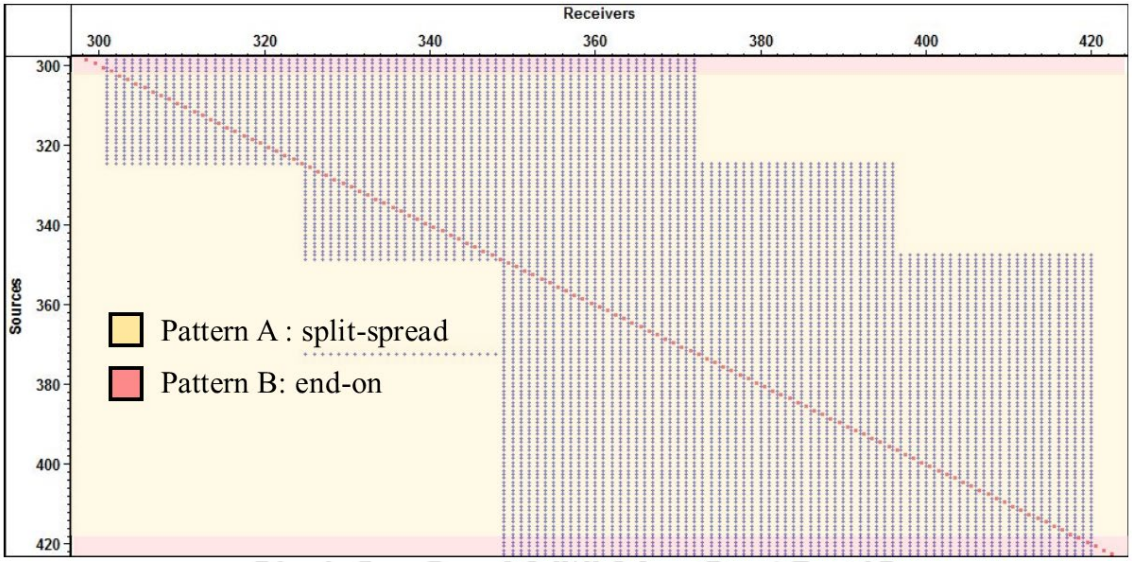

Figure 2.17 shows stacking chart of survey Line MO-4 (red and blue dots are shot and receiver locations) with split-spread configuration (yellow zone) and end-on configuration (light-red zone).

2.4. Seismic Reflection Processing

Generally, the objectives of seismic data processing can be summarized into two main topics, to enhance the signal to noise ratio (S/N) and obtain seismic sections, from which the information of subsurface can be interpreted. The first part is involving the preparation of field data for signal to noise ration enhancing, such as data editing, amplitude recovery, static correction, and wide range bandpass filter. After that, the parameters that used for S/N enhancing will be tested such as bandpass filter and deconvolution. Then, the velocity information is acquired from velocity analysis for NMO correction. The final seismic cross-section or seismic profile is the result from CMP data stacking process. By using the shot gather example from survey data of the survey Line MO-2, this toping will show example solutions of key processing steps.

2.4.1. Geometry setting

This processing is started in Vista 5.5 program. The seismic data are converted from SEG-2 format into Vista's file format. The coordinates of source and receiver locations were input and carefully quality checked on header. The precision of location base on the information available from the observers' log (field note) and DGPS. Seismic processing

conventionally is done in common midpoint (CMP) gather (Figure 2.9) which the seismic traces should have the same reflected point from difference shot and receiver base on a straight line. However, the seismic reflection surveys were conducted along existing crooked lines. Resulting in the common midpoint distribute outside of the survey line. Therefore, a surface line is drawn among the CMP point along the survey line (the red dot line in Figure 2.18). Then the bin area is construct perpendicular to the surface line with an area of 1.96×20 m^2 to cover the group of nearby midpoints. The number of traces which have midpoints available within the bins, are combined as the fold coverage (Figure 2.19).

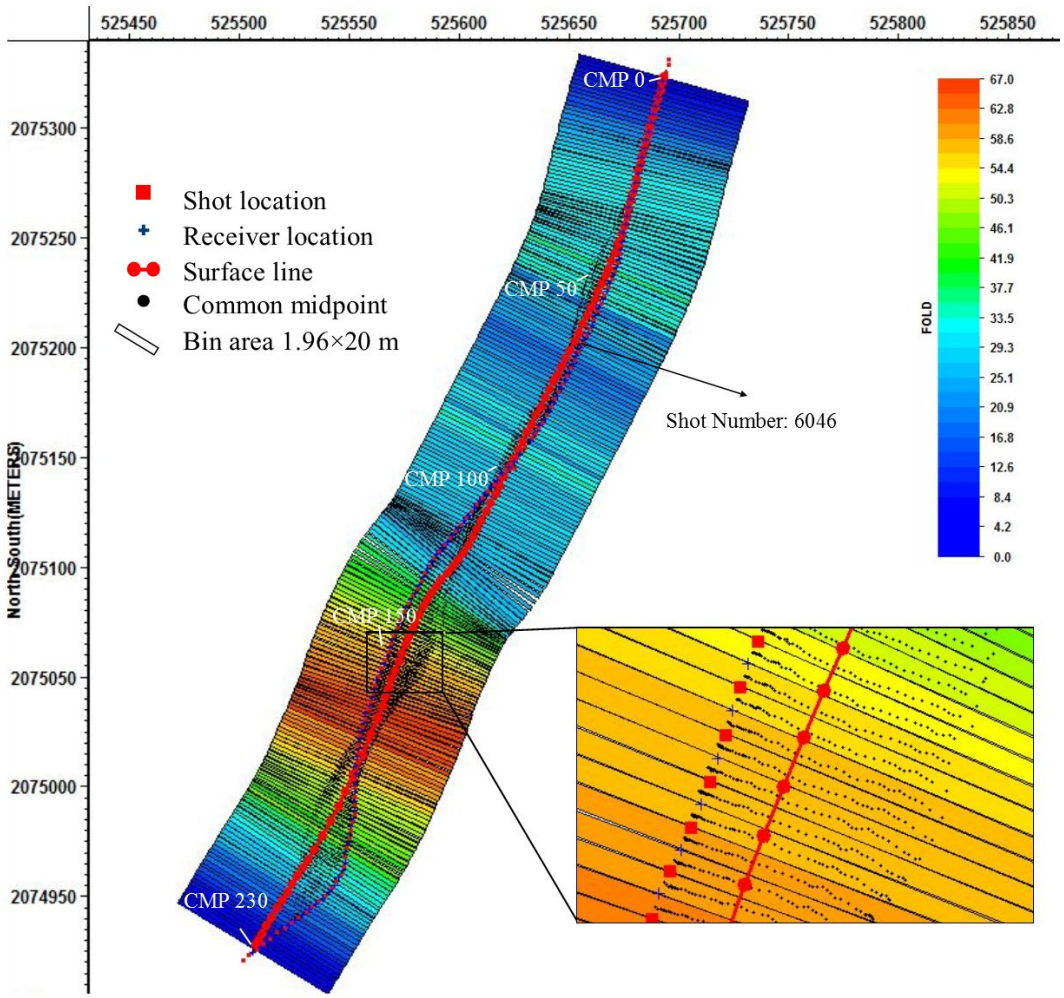

Figure 2.18 displays geometry setting of Line MO-2. The receiver and shot locations represent by blue plus and red square. The surface line is in red-circle line constructed base on the straight-line. The black dots are common midpoints. The bins are shown in rectangular area with 1.96×20 m^2 and color bar represents the fold coverage.

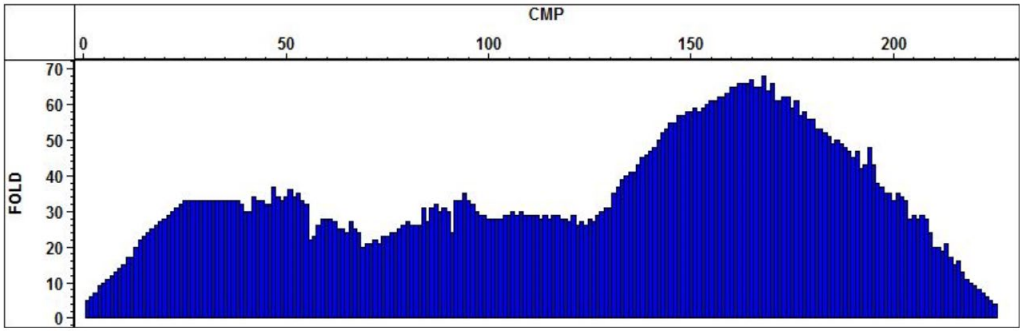

Figure 2.19 exhibits the total fold coverage of each CMP from Line MO-2

2.4.2. Trace editing, amplitude recovery and static correction

The example of raw shot data number 6046 is shown on Figure 2.20a with average amplitude spectrum in Figure 2.20b. The raw shot data directed from field survey do not display any interested seismic event because of the large-scale energy of surface wave.

The bad traces should be removed from the input data. The cross-plot correlations of trace statistic in shot gather was analyzed with 3 techniques for quality control of seismic traces, offset versus RMS-amplitude, offset versus maximum frequency, and offset versus exponential amplitude decay. The trace statistics values that are far from main trend or abnormal unexpected values should be examined and killed if necessary.

The main attenuations of seismic signal are due to spherical divergent, scattering, and absorption. This survey line used exponential function technique. The parameter of exponential function is 0.5 to recovery weak seismic signal that reduces by time. The raw data were tested until the amplitude is balanced.

For static correction, this involves the computation and removal of the effect of different source and receiver elevation. Therefore, elevation static correction is calculated to adjust the source and receiver to a common datum base on first arrival time. This study used floating datum with radial 200 m smoothing.

The directed wave, reflected wave, air wave, and ground roll are recognized and indicated in shot record with velocity information in red, yellow, green, and blue lines, respectively (Figure 2.21). The velocity of weathered sediment layer is approximately 600 m/s measured from directed wave arrival time (red line). The second reciprocal slope of the first arrival time is the refracted wave represented in yellow line which indicates the velocity of second layer

as 4000 m/s. The surface wave and air blast can also be indicated with an apparent velocity about of 200 m/s and 330 m/s, respectively. The thickness of sediment layer can be determined that is about 5-10 m on Figure 2.22. In addition, the seismic reflection resolution depended on the velocity and frequency of seismic signal. The sediment layer (first layer) has a velocity of about 600 m/s and a dominant frequency of 30 Hz. It can assume a wavelength about 20m. The vertical resolution can be approximated from a half of the wavelength, therefore, the vertical resolution is limited about 10 m. The sediment layer that examined from directed and refracted wave is about 5-10 m which less than vertical resolution consequence the sediment layer could not detected by reflection seismic.

Moreover, Figure 2.20b displays the average amplitude spectrum of the shot number 6046 that shows the frequency content of seismic signal ranges approximately from 20 Hz to 100 Hz. The high frequency noise that recorded from field survey should be remove before deconvolution step. To remove unnecessary high frequency noise, the wide range bandpass filter was applied with 10-20-200-250 Hz frequency band selected based on its amplitude spectrum. The objective of this filter is to remove noise that is not exist in the wanted signal frequency range. The shot number 6046 processed with geometry setting, amplitude recovery and scaling for amplitude blanching, static correction, and then broaden bandpass filter, 10/20-200/250 Hz, is shows in Figure 2.20c with its amplitude spectrum in Figure 2.20d. The amplitude of shot record, now, has been compensated thus it shows the pattern of seismic events.

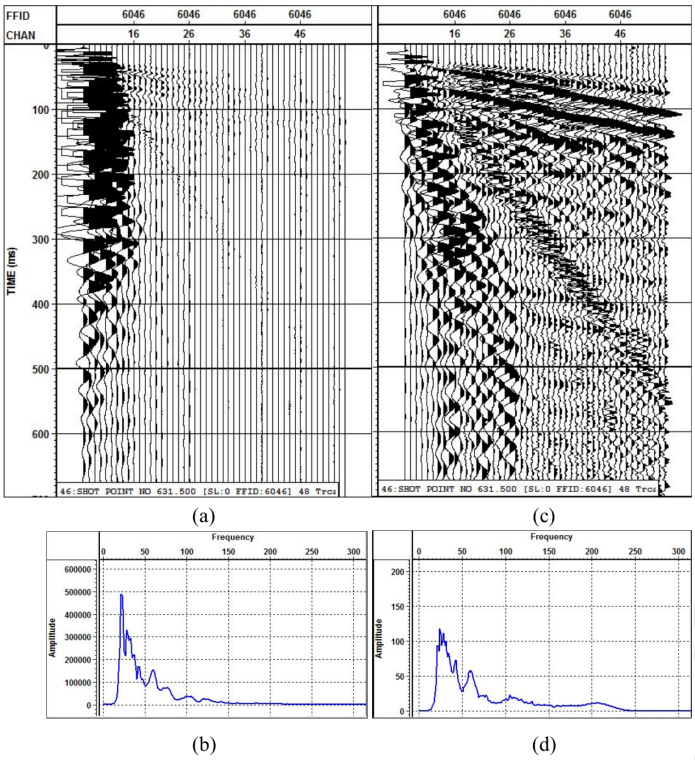

Figure 2.20 shows example shot gather number 6046, (a) raw shot record with its average amplitude spectrum (b) and (c) shot gather after geometry setting, static correction, amplitude scaling and recovery with exponential constant 0.5 to compensate for attenuation loss and bandpass filter 10-20-200-250 Hz with its average amplitude spectrum in (d).

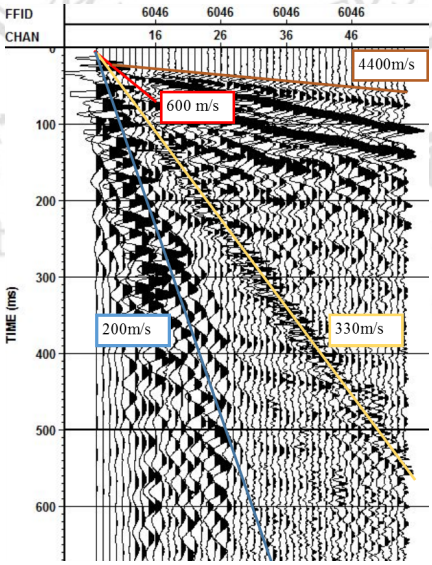

Figure 2.21 displays example seismic shot record number 6046 from Line MO-2 with amplitude balancing. The directed wave, reflected wave, air wave, and ground roll are indicated with velocity information in red, yellow, green, and blue lines, respectively.

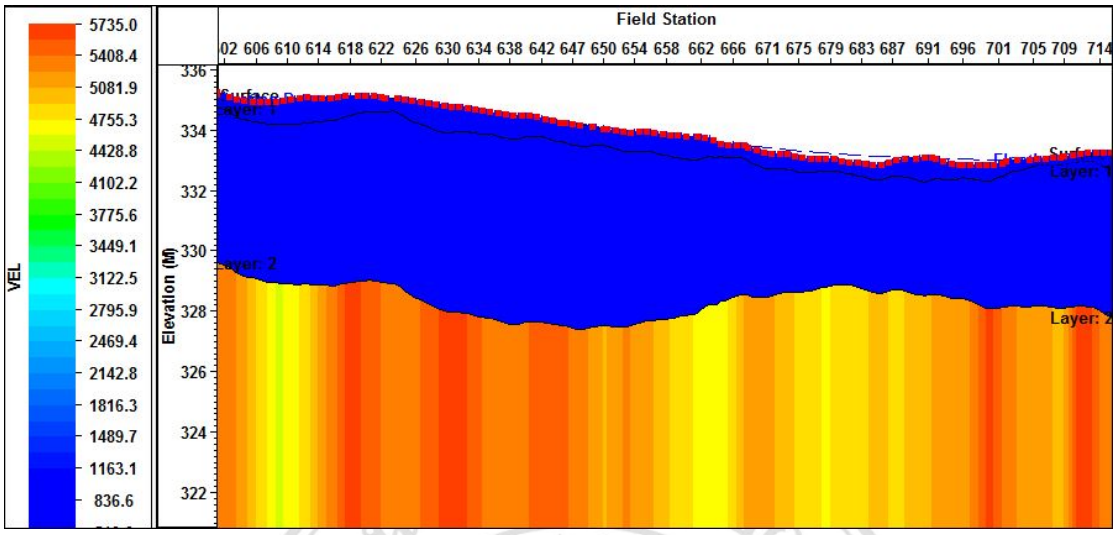

Figure 2.22 displays velocity model of Line MO-2 determined from first arrival time. The velocity values are shown in m/s unit

2.4.3. Frequency filter analysis

The frequency range of seismic data considered base on its average amplitude spectrum are between 20 to 100 Hz (Figure 2.20d). The optimum bandpass frequency filter is determined by analyzing the frequency content of the signal.

The low-cutoff frequency was tested first by fix the high frequency cutoff at 100-150 Hz and varies the low frequency cutoff from 10 Hz to 20Hz. The designed bandpass filters for testing low cutoff frequency are 10-15-100-150 Hz, 15-20-100-150 Hz, and 20-25-100-150 Hz displayed in the top three of Figure 2.23. From that, bandpass filter at 10-15-100-150 Hz and 15-20-100-150 Hz are chosen because they show the reflector clearer whereas bandpass filter 20-25-100-150 Hz shows un-cleared reflector at about 220 ms. Therefore, the low-cutoff frequency filter are started at 10-20 Hz.

After this, the high-cutoff frequency was tested by fix the low frequency cutoff at 10-20 Hz and varies the high frequency cutoff. The designed bandpass filters for testing high cutoff frequency are 10-20-80-110 Hz, 10-20-90-120 Hz, and 10-20-100-120 Hz displayed in the bottom three pictures of Figure 2.23. From those pictures, they do not show any difference in each filter. Therefore, the high-cutoff frequency, 90-120 Hz, was selected base on original amplitude spectrum of shot record. The bandpass filter that will used to filter out some frequency contents in the seismic record is10-20-90-120 Hz.

According to the frequency filter analysis, frequency filter is tested before deconvolution was applied. However, the frequency filter will be applied after performing deconvolution because the deconvolution will recover all the frequency content of seismic data, both signal and noise amplitude spectrum are boosted up.

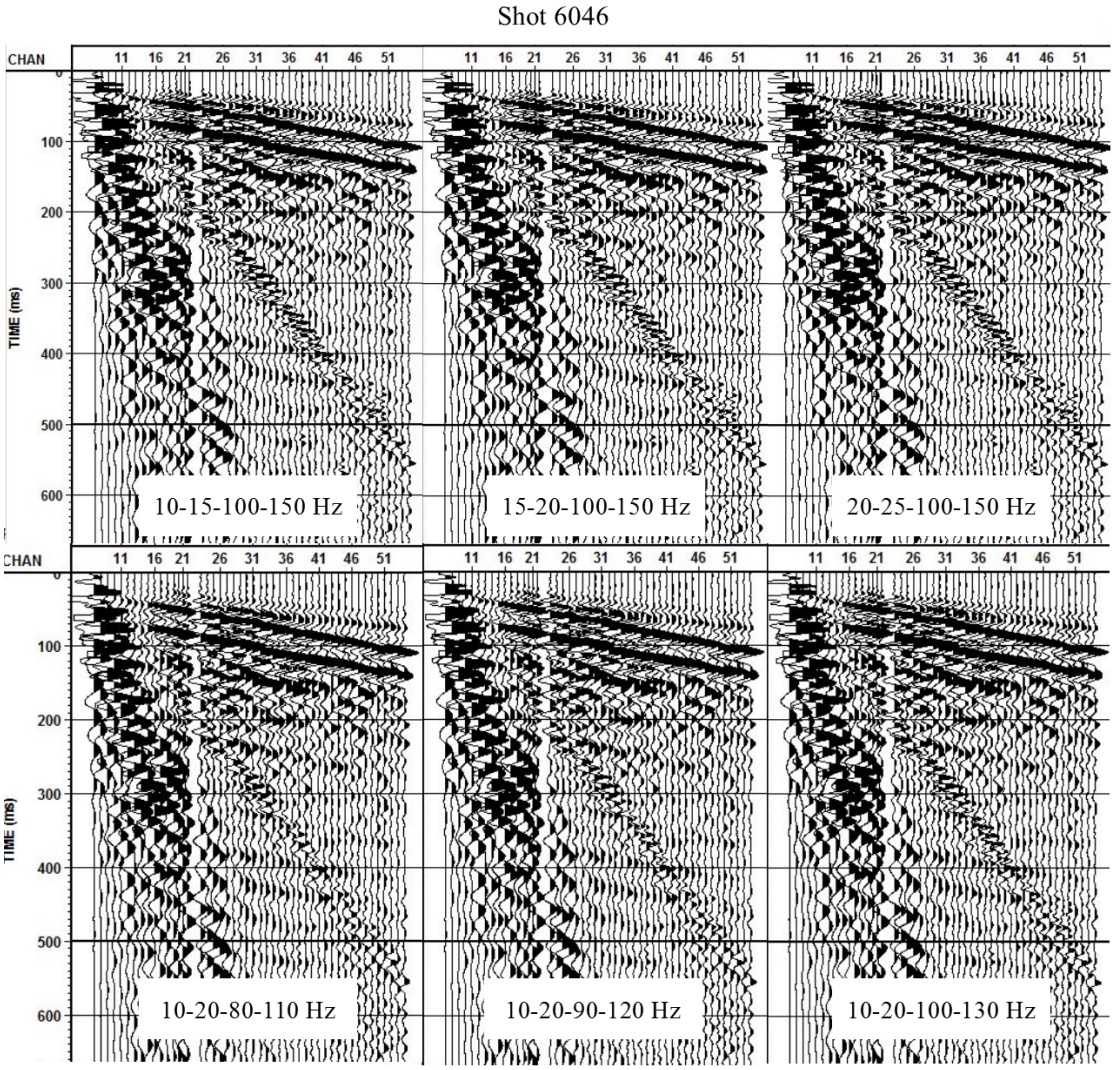

Figure 2.23 demonstrates bandpass frequency analysis of shot number 6046

2.4.4. Deconvolution parameter testing

There are two main parameters of surface consistent deconvolution which are operator length and predictive lag. The best operator for unknown source wavelet are defined from autocorrelation of shot record (Figure 2.24). The operator length is tested by varies from 40 to 120 ms because it is a range of signal which gradually disappear. When the operator

length is tested the predictive lag is fixed at 21 ms which is the second zero crossing time. The operator lengths are tested at 40, 60, 80, 100, and 120 ms, each of deconvolution testing demonstrate on Figure 2.25. The operator length at 80 ms is chosen because it shows reflector clearly. Later, the operator length is fixed at 80 ms and the predictive lag is tested by varying from 12 to 30 ms. The predictive lags are tested at 12, 18, 21 (2nd zero crossing), 24, and 30 ms. The predictive lag at 21 ms is chosen because the reflectors are observed clearly. Therefore, the optimum deconvolution parameters are operator length of 80 ms and predictive lag at the 2nd zero crossing (21 ms). Figure 2.25 shows the final deconvolution using those optimum parameters.

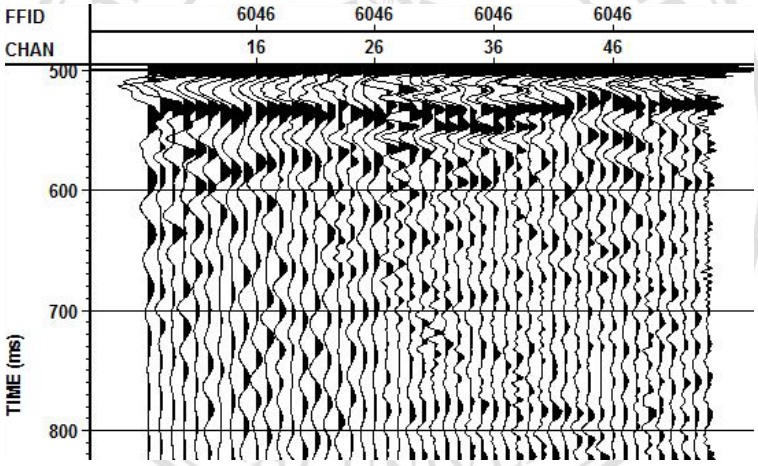

Figure 2.24 is the autocorrelation of shot number 6046 showing the second zero crossing time at about 21 ms.

Shot 6046

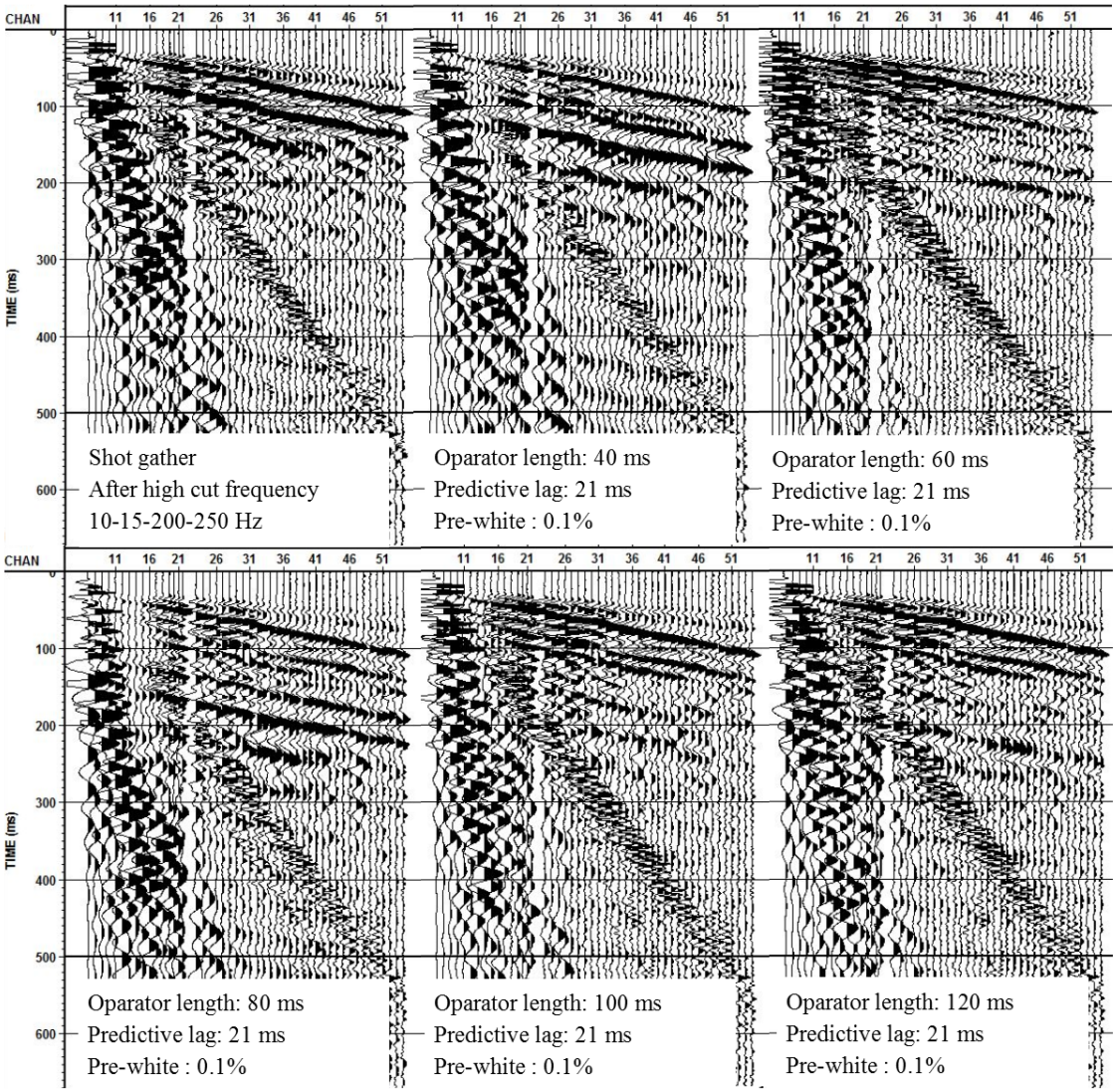

Figure 2.25 demonstrates deconvolution operator length testing with the same predictive lag of 21 ms.

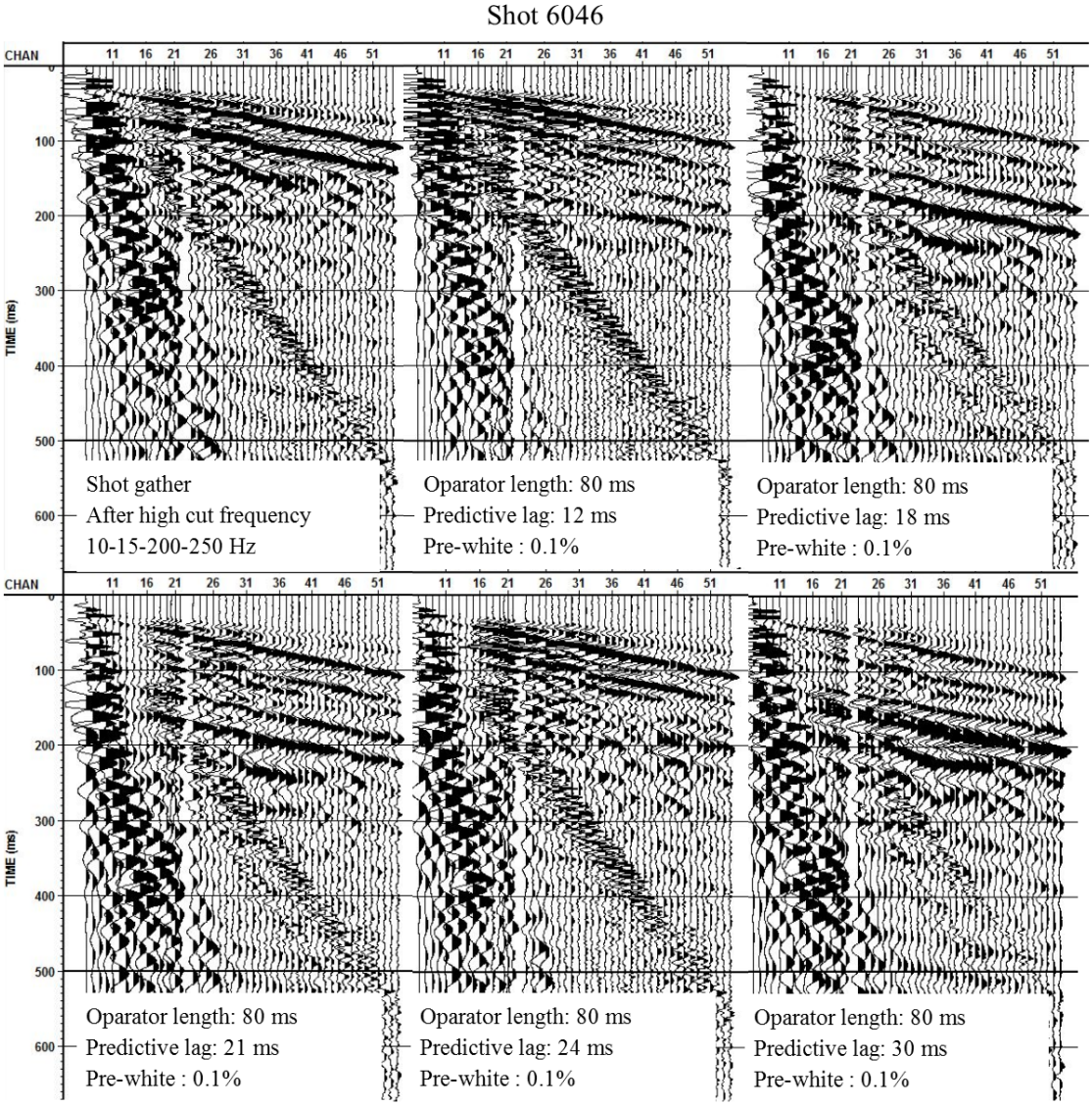

Figure 2.26 demonstrates deconvolution predictive lag testing with the same 80 ms operator length.

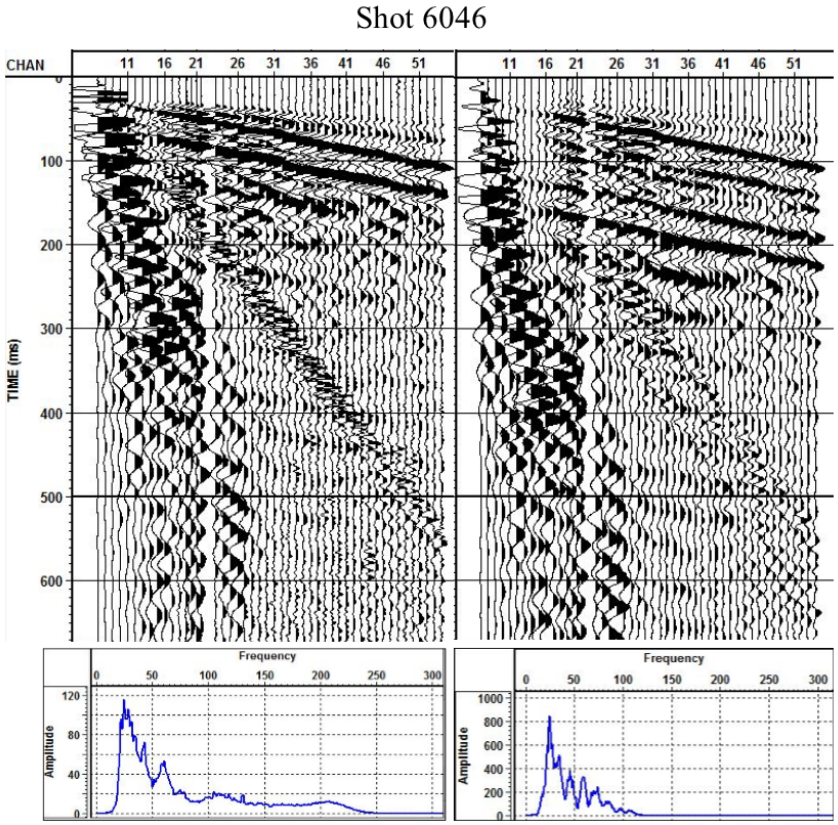

Figure 2.27 displays the signal entrancing of (left) example shot after frequency filter 10-20-200-250 and then (right) after surface consistent deconvolution with operator length 80 ms and predictive lag 21 ms follow by 10-20-90-120 bandpass filter and mean scaling.

2.4.5. Velocity analysis and NMO correction

Velocity analysis is the process step that attempts to discover the stacking velocity for each hyperbola event. Seismic shot gathers were rearranged into common-mid-point (CMP) gathers for determining the suitable stacking velocity model. By doing that, the $t - x$ domain of a CMP record will be transformed into velocity semblance image (Figure 2.28a) and a group of nearby CMP gather was simultaneously applied the constant velocity stack (CVS) (Figure 2.28c). Velocity analysis was performed manually and picking velocity by inter-panel active of semblance panel, constant velocity stack and CMP gather with offset spacing. Finally, this method defied possibly velocity model at each CMP gather location that could image shallow event of subsurface. Figure 2.29 presents the stacking velocity models from velocity analysis of survey Line MO-2. The color bar indicates stacking or average velocity values.

During velocity picking and flattening CMP gathers, it is noticeable that the gathers are flattening at the near offset but this is not for a case of far offset. The NMO corrected data were stretched due to the different time move-out which is larger at far offset and shallow time. Therefore, the CMP muting after NMO correction must be assigned to remove NMO stretch at far offset (Yilmaz, 2001).

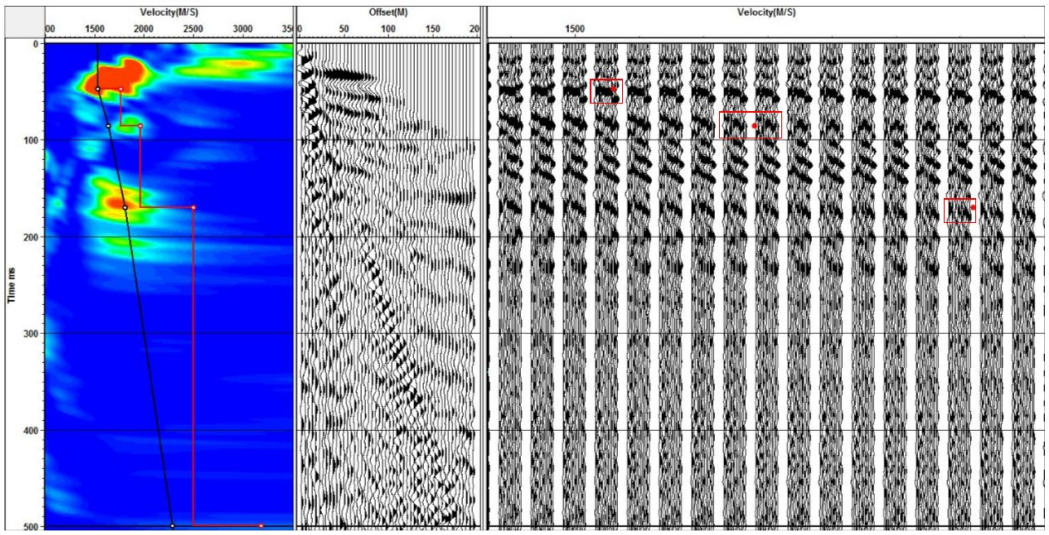

(a) (b) (c)

Figure 2.28 demonstrates velocity analysis of CMP number 90 from Line MO-2, (a) semblance, (b) NMO corrected gather applied by picking velocity function, and (c) constant velocity stack panel, CVS.

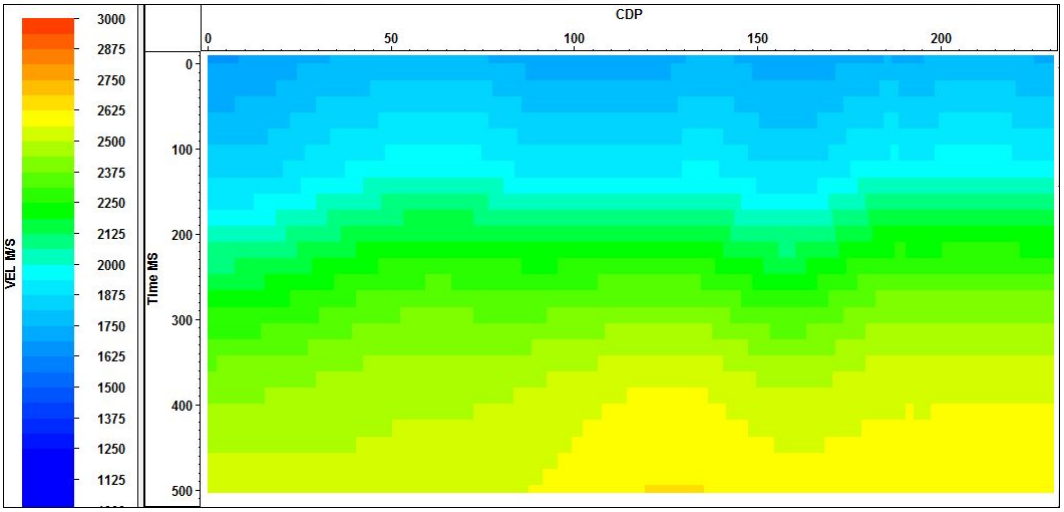

Figure 2.29 shows the stacking velocity models from velocity analysis of Line MO-2.

2.4.6. Processing summary parameters and final seismic cross-sections

The four seismic survey lines are processed by using mostly the same processing workflow. However, the parameters in each step are tested individually. The example pictures from some processing steps of each line survey are displayed in Appendix B. The survey configuration is an important factor that control the processing workflow. Split-spread configuration contains more ground roll energy than end-on configuration because the energy of ground roll is stronger near shot point location. Line MO-1 and MO-2 which have more end-on pattern than split-spread pattern in acquisition, use the same workflow. Whereas, Line MO-3 and MO-4 which mostly have split-spread configuration in acquisition use the same processing workflow except for deconvolution and FK filtering procedures. Line MO-3 uses only surface consistence deconvolution while Line MO-4 uses predictive deconvolution and FK filtering due to that split-spread configuration in acquisition containing more ground roll energy. The ground roll has large amplitude and low frequency which will almost cover any signal especially the signal correspond to reflection on the traces of near offset. The various techniques in the workflow could not completely remove ground roll energy then the bottom mute is applied on Line MO-3 and MO-4. The processing workflows are summarized in Table 2.3, Table 2.4, Table 2.5, and Table 2.6 for survey Line MO-1, MO-2, MO-3, and MO-4, respectively. There is no diffraction energy observed in the final stacked sections. Therefore, the migration is excluded from the processing workflow. The solution from seismic data processing are the final stacked sections or seismic profiles. Figure 2.30, Figure 2.31, Figure 2.32, and Figure 2.33 display the survey results of Line MO-1, MO-2, MO-3, and MO-4, respectively. The top picture shows CMP fold coverage, the CMP that has greater number of fold coverage has more reliability in the interpretation.

Table 2.3 reviews the processing steps and parameters applied for Line MO-1.

Step Line	Parameters
1) Input Geometry	Read SEG-2 data
2) Edit trace	Kill bad traces
3) Recovery amplitude and scaling	Exponential power, $n = 1$ RMS scaling factor = 1
4) Static correction	Elevation static, Floating datum weathered velocity 600 m/s Replacement velocity 4000 m/s
5) Frequency filter	Bandpass filter: 10-20-200-250 Hz
6) Deconvolution	Surface consistence deconvolution Operator length 80 ms and lag 12 ms
7) Frequency filter	Bandpass filter: 10-20-90-120 Hz
8) CMP sorting	Total 515 CMPs
9) Velocity analysis	Velocity picking 25 CMPs
10) NMO correction	Apply NMO with stretch mute: 95%
11) Stacking	

Table 2.4 reviews the processing steps and parameters applied for Line MO-2.

Step	Parameters
1) Input Geometry	Read SEG-2 data
2) Edit trace	Kill bad trace
3) Recovery amplitude	Exponential power, $n = 0.5$
4) Static correction	Elevation static, Floating datum weathered velocity 600 m/s Replacement velocity 4000 m/s
5) Frequency filter	Bandpass filter: 10-20-200-250 Hz
6) Deconvolution	Surface consistence deconvolution Operator length 80 ms and lag 21 ms (2nd zero crossing)
7) Frequency filter	Bandpass filter: 10-20-90-120 Hz
8) CMP sorting	Total 230 CMPs
9) Velocity analysis	Velocity picking 14 CMPs
10) NMO correction	Apply NMO stretch mute: 95%
11) Stacking	

Table 2.5 reviews the processing steps and parameters applied for Line MO-3.

Step Line	Parameters
1) Input Geometry	Read SEG-2 data
2) Edit trace	Kill bad trace
3) Recovery amplitude	Exponential power, $n = 1$
4) Static correction	Elevation static, Floating datum weathered velocity 600 m/s Replacement velocity 4000 m/s
5) Frequency filter	Bandpass filter: 10-20-200-250 Hz
6) Deconvolution	Surface consistence deconvolution Operator length 80 ms and lag 12 ms
7) Frequency filter	Bandpass filter: 10-20-90-120 Hz
8) Bottom mute	Slope 150 m/s
9) CMP sorting	Total 248 CMPs
10) Velocity analysis	Velocity picking 6 CMPs
11) NMO correction	Apply NMO stretch mute: 95%
12) Stacking	

Table 2.6 reviews the processing steps and parameters applied for Line MO-4.

Step Line	Parameters
1) Input Geometry	Read SEG-2 data
2) Edit trace	Kill bad trace
3) Recovery amplitude	Exponential power, $n = 0.25$
4) Static correction	Elevation static, Floating datum weathered velocity 600 m/s Replacement velocity 4000 m/s
5) FK filter	Velocity filter 70-500 ms
6) Frequency filter	Bandpass filter: 10-20-200-250 Hz
7) Deconvolution	Predictive deconvolution operator Operator length 80 ms and lag 2nd zero crossing
8) Frequency filter	Bandpass filter: 10-20-90-120 Hz
9) Bottom mute	Slope 150 m/s
10) CMP sorting	Total 239 CMPs
11) Velocity analysis	Velocity picking 21 CMPs
12) NMO correction	Apply NMO stretch mute: 95%
13) Stacking	

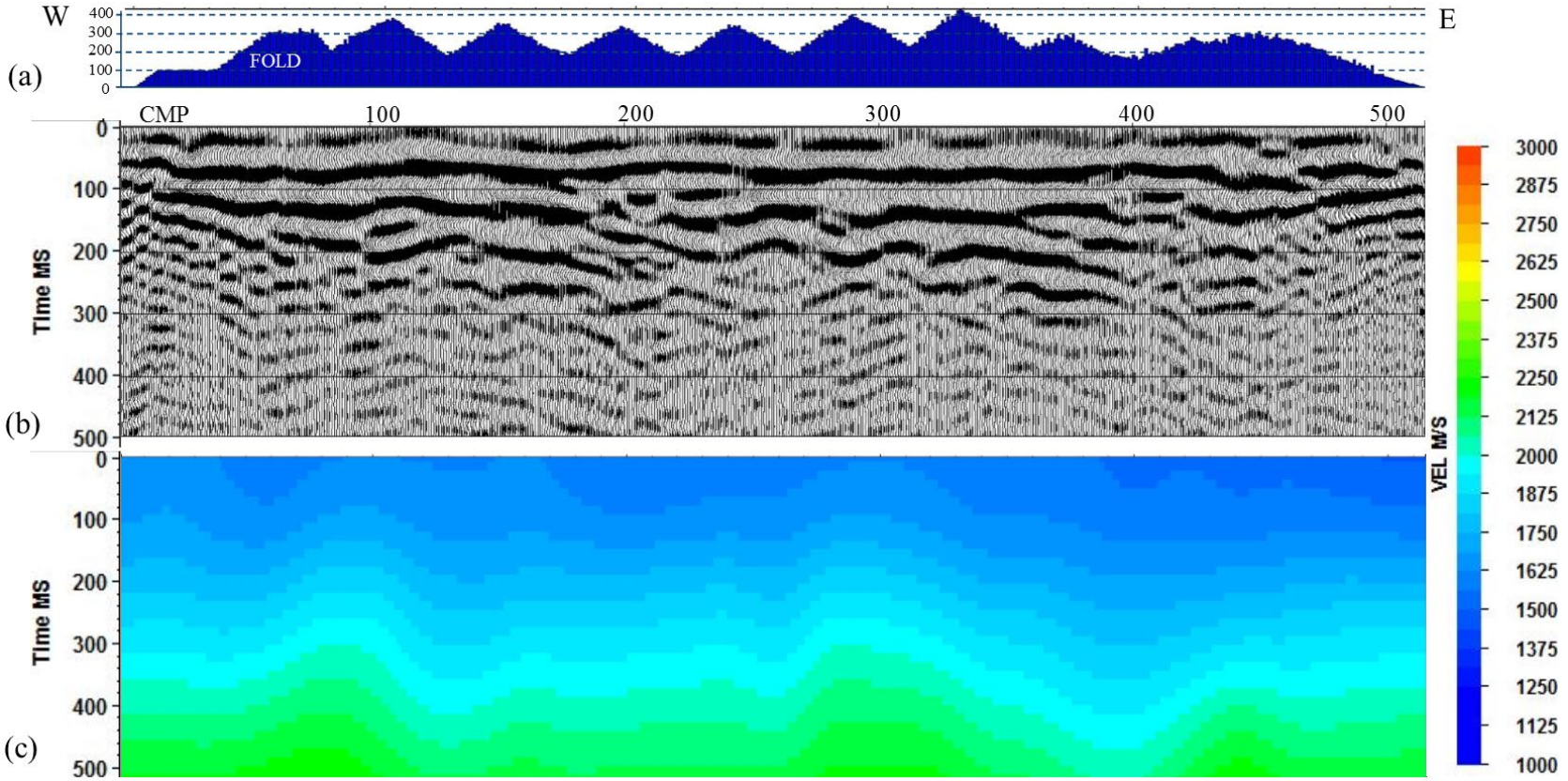

Figure 2.30 shows (a) fold coverage in each CMP, (b) final stacked section and (c) stacking velocity models from velocity analysis of Line MO-1

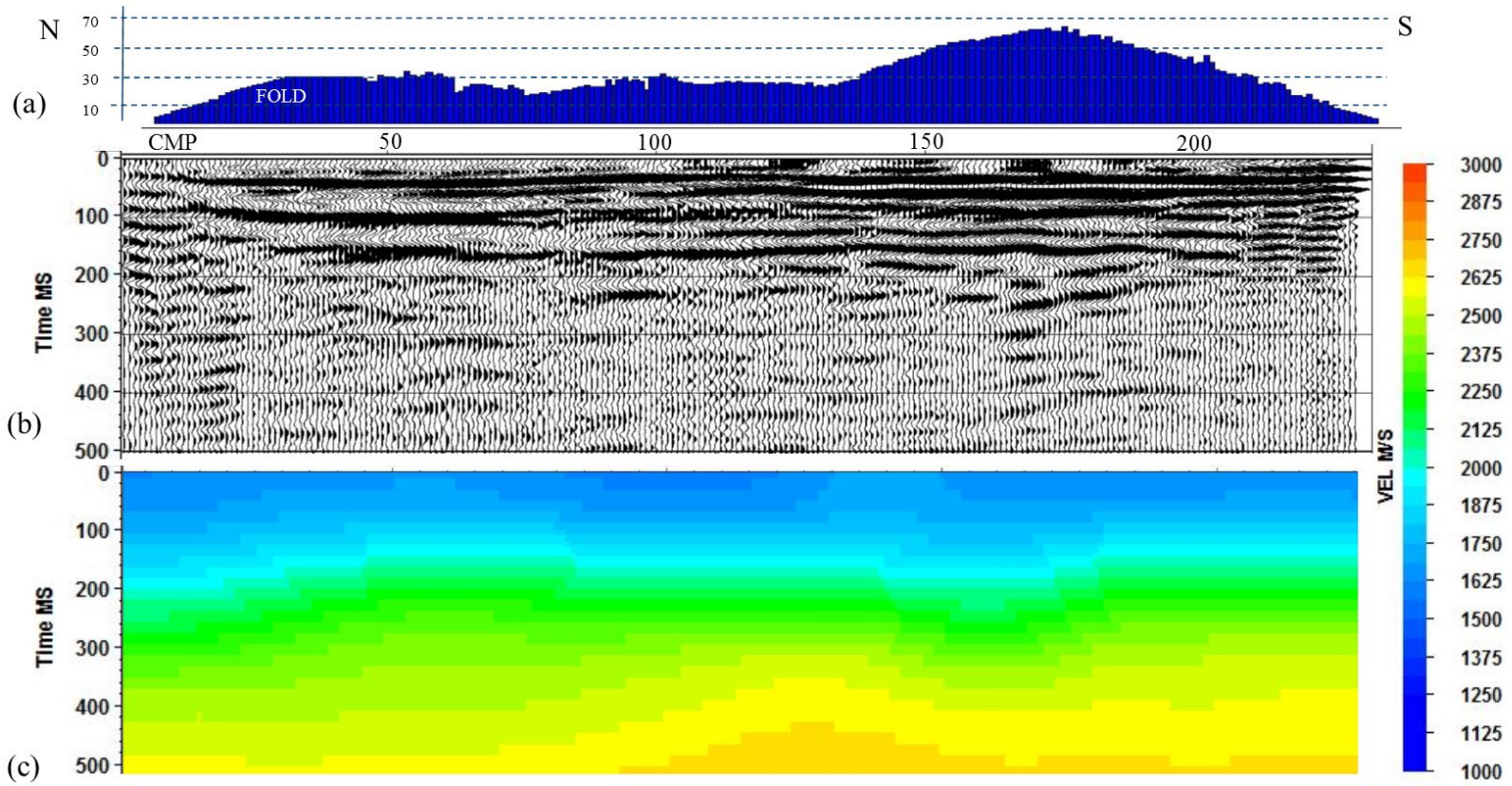

Figure 2.31 shows (a) fold coverage in each CMP, (b) final stacked section and (c) stacking velocity models from velocity analysis of Line MO-2

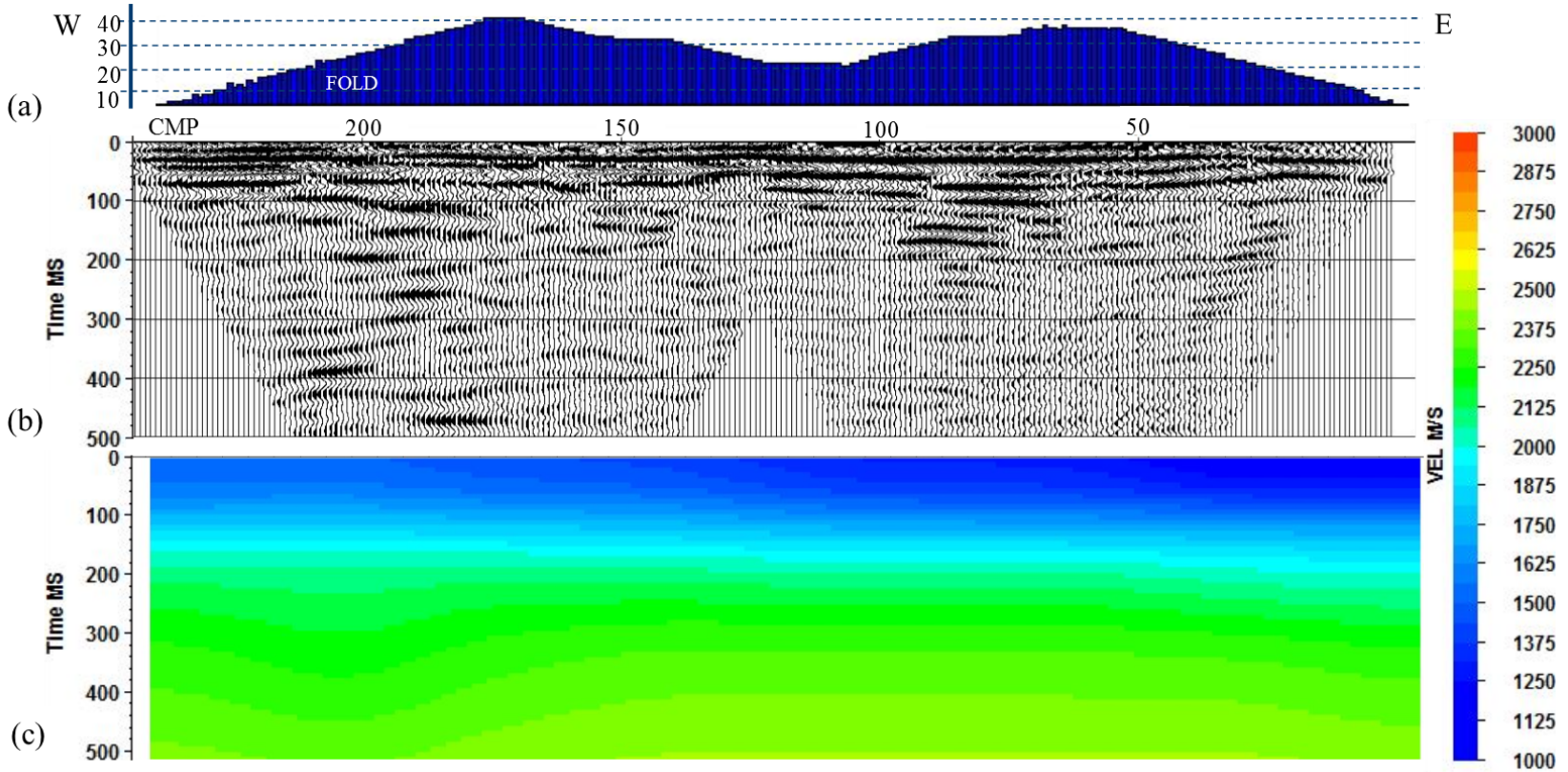

Figure 2.32 shows (a) fold coverage in each CMP, (b) final stacked section and (c) stacking velocity models from velocity analysis of Line MO-3

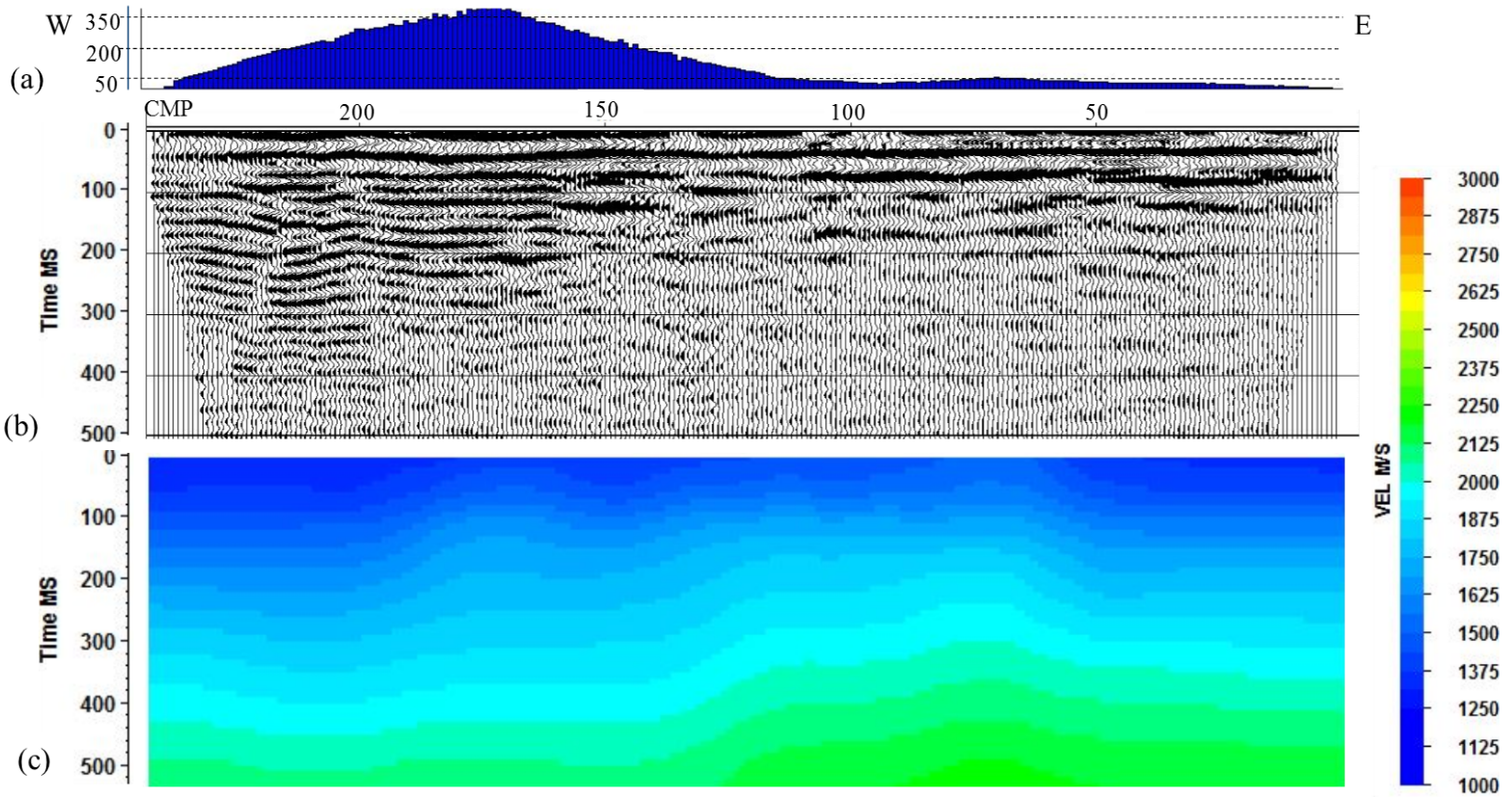

Figure 2.33 shows (a) fold coverage in each CMP, (b) final stacked section and (c) stacking velocity models from velocity analysis of Line MO-4

2.5. Seismic data interpretation

The objective of seismic survey is to find the geological structure of the investigation area. Seismic signal which shows on seismic trace, having characteristics base on the different of lithology layers (boundary). After data processing was done, seismic data were interpreted to identify the shallow subsurface structure base on the seismic signal characteristics. There are three mains characteristics, amplitude, continuity, and spacing that used as the guideline for interpretation.

Reflection amplitude explains the strong of reflection peak and is dependent on the acoustic contrast between an upper and lower of the reflector. Reflection continuity describes the lateral variation of lithology layer due to the pattern and structure of geological term. The last characteristic is reflection spacing define the frequency of reflector per unit of time due to the thickness of lithology and stratigraphy. Therefore, the mains characteristics of reflector in this study were used for interpretation as follow.

The reflection seismic profiles MO-1 (Figure 2.34a) and MO-2 (Figure 2.35a) summarize into three main seismic reflectors. There are upper reflector (USR), middle reflector (MSR), and lower reflector (LSR) that represented with blue, green, and yellow lines, respectively. Whereas, the reflection seismic profiles MO-3 (Figure 2.34b), and MO-4 (Figure 2.34c) summarize into two main seismic reflectors which are upper reflector (USR), middle reflector (MSR).

The USR reflector presents characterization which is high continuity, high amplitude and nearly horizontal pattern with travel time about 35-40 ms and average velocity approximate 1500-1600 m/s. The MSR reflector shows high amplitude, moderate continuity, and nearly irregular pattern with travel time about 70-100 ms and average velocity approximate 1600-1700 m/s. The deepest reflector, LSR, shows high amplitude, moderate continuity, and horizontal pattern with travel time about 120-160 ms and average velocity approximate 1750-1800 m/s. The information from interpretation are listed in Table 2. of each reflector.

Table 2.7 shows the interpretation detail on three reflectors with approximate two-way travel time, average stacking velocity or approximate V_{rms}, and depth.

Reflector	Indicator	MO-1	MO-2	MO-3	MO-4
USR	Time (ms)	35-40	35-40	25-30	40
	V_{rms} (ms)	1550	1600	1550	1500
	Depth (m)	27-31	28-32	19-23	30
MSR	Time (ms)	85-95	85-100	70-80	70-80
	V_{rms} (ms)	1650	1700	1600	1600
	Depth (m)	70-78	72-85	56-64	56-64
LSR	Time (ms)	110-120	120-160	-	-
	V_{rms} (ms)	1750	1800	-	-
	Depth (m)	96-105	108-144	-	-

According to Table 2.7, the reflector USR, MSR, and LSR separate four major seismic units. From upper to lower, the Upper unit (UU) shows interval velocity about 1500 m/s with 30 m average thickness. The UU unit is underlain by First Mid unit (MU1). The MU1 has interval velocity about 1800 m/s with an average thickness of 40 m, it is underlain by Second Mid unit (MU2). The MU2 has interval velocity 1900 m/s with 40 m average thickness. The last unit is underling MU2 which is Lower unit (LU) has interval velocity higher than 2100 m/s.

The results from refraction method which examined the directed and refracted waves show that the sediment layer has 5-10 m average thickness (Figure 2.22). On the other hand, seismic reflection profiles were interpreted into four units, sediment layer which is topmost layer could not be detected on seismic profiles. Hence, the interval velocity of UU unit is resulted from the average velocity of sediment and basaltic layers. Because the seismic reflection resolution depended on the velocity and frequency of the signal. The sediment layer has velocity of about 600 m/s and dominant frequency of 30 Hz. Then, the wavelength is about 20 m. The vertical resolution can be approximated from a half of the wavelength, hence, the vertical resolution is limited about 10 m. The thickness of sediment layer less than vertical resolution. Therefore, the results of electrical resistivity

and multichannel analysis surface wave (MASW) surveys were required to support the seismic reflection interpretation for the top layer. The previous resistivity and MASW data are overlapped with seismic profile MO-2 so that the shallow structure are interpreted base on all available information on survey Line MO-2. The acquisition and processing of resistivity and MASW method are summarily descripted in Appendix C.

The results from electrical resistivity and MASW surveys from Line MO-2, the true electrical resistivity model and S-wave velocity model, show detail of the upper part geological structure. The true electrical resistivity model in Figure 2.35b displays three nearly horizontal layers with the maximum investigation depth of about 70 m. Whereas, the S-wave velocity model in Figure 2.35c explores more detail of near surface layers with the maximum investigation depth of about 30 m. The top soil layer with low resistivity less than 50 ohm.m and low S-wave velocity less than 400 m/s has the thickness approximately 10 m corresponding to low P-wave velocity of 600 m/s (directed wave, Figure 2.21) which could not detect by seismic reflected wave. However, from the first arrival time in shot record (Figure 2.21), there is the shallow high P-wave velocity layer (about 4400 m/s) that might be corresponding to the unit UU indicated in Figure 2.35. The corresponding to the UU unit in seismic section has the estimated thickness of 30 m with high resistivity range from 50 to 600 ohm.m. From MASW, the UU unit also has high S-wave velocity approximately might higher than 2000 m/s in the southern part of Line MO-2 which could related to the hard rock layer. The deepest layer from electrical resistivity model is corresponding to the MU1 unit of seismic section and has resistivity range about 35-200 ohm.m.

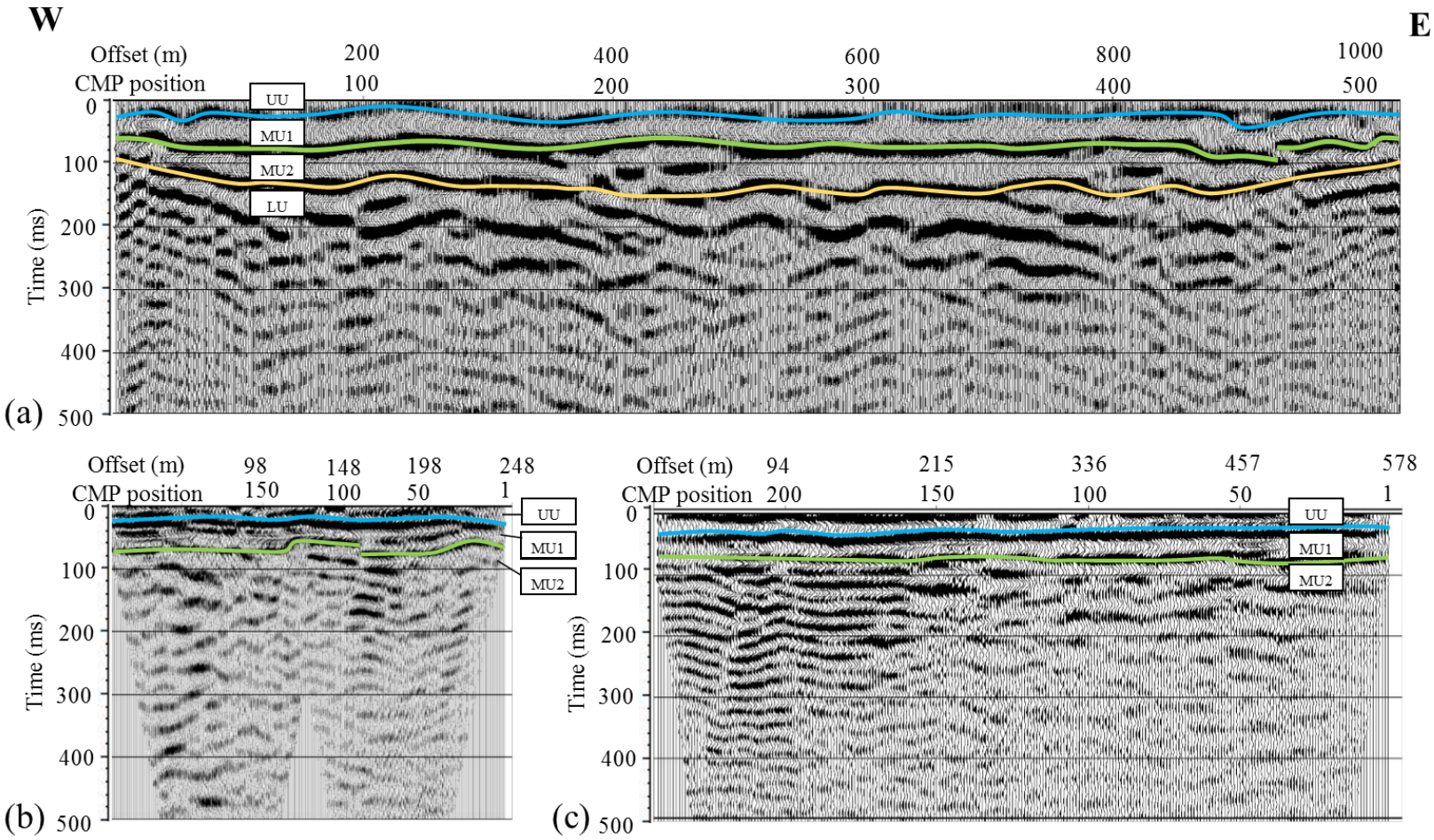

Figure 2.34 shows final stacked section of line survey MO-1 (a), MO-3 (b), and MO-4 (c) with interpretation, blue, green, and yellow line are upper (USR), middle (MSR), and lower (LSR) reflectors, respectively.

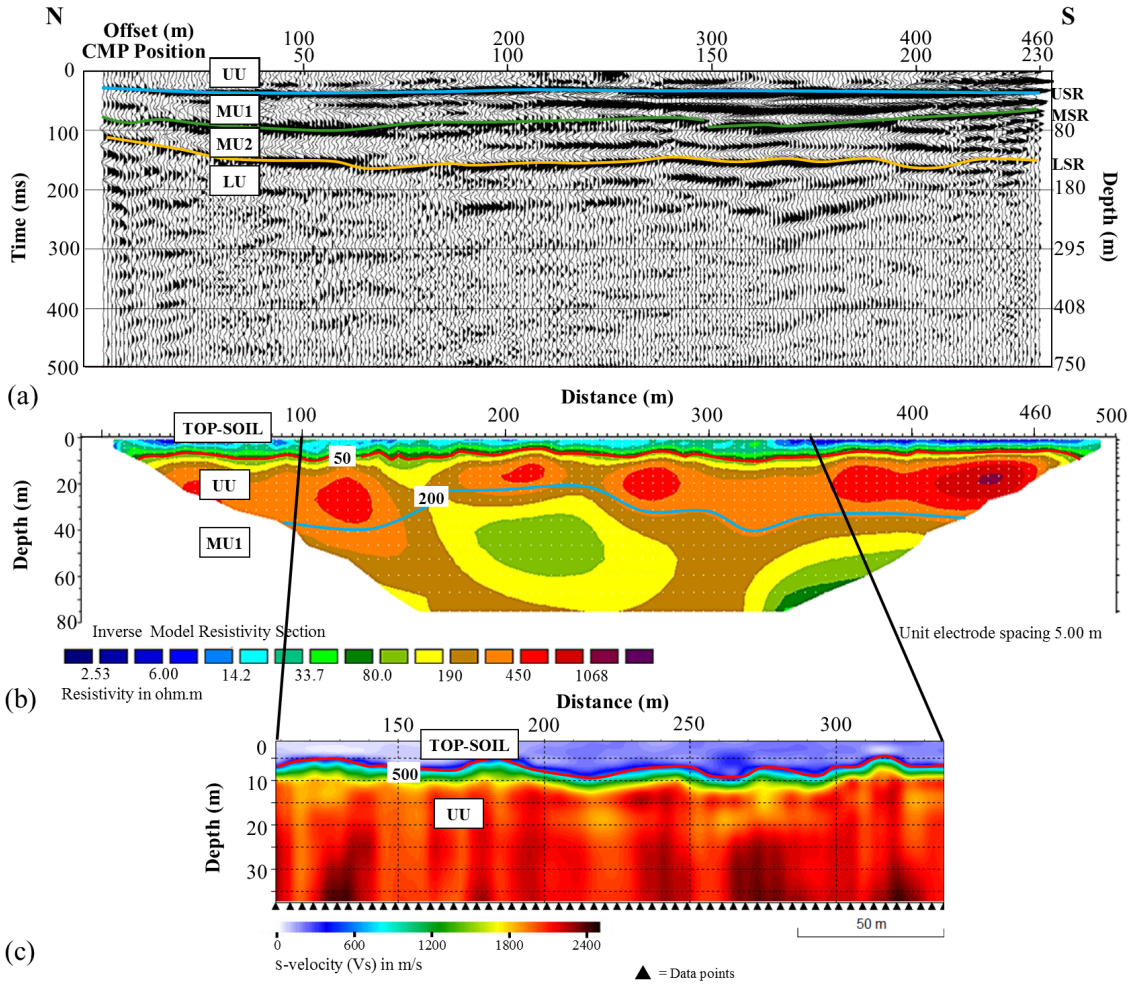

Figure 2.35 displays (a) interpreted seismic reflection section, (b) true electrical resistivity model and (c) S-wave velocity model from line survey MO-2.